Research Square

Preprints are preliminary reports that have not undergone peer review.
They should not be considered conclusive, used to inform clinical practice,
or referenced by the media as validated information.

Ligilactobacillus salivarius enolase is an oxytocin-like systemic signal and it is reduced in children with autism spectrum disorder

Serguei Fetissov

Serguei.Fetissov@univ-rouen.fr

University of Rouen Normandy https://orcid.org/0000-0002-2491-4945

Emilie Lahaye

Rouen University

Benjamin Thomas

University of Rouen Normandy

Marion Nicol

Rouen University

Alizée Lanon

MetaGenoPolis, INRAE

Philippe Chan

University of Rouen

Lisa Wallart

University of Rouen Normandy

Ilaria Olivito

University of Rouen Normandy

Amaël Robert

University of Rouen Normandy

Karthi Duraisamy

University of Rouen Normandy

Benjamin Lefranc

INSERM

Jérôme Leprince

https://orcid.org/0000-0002-7814-9927

Arnaud Arabo

University of Rouen Normandy

Dario Siniscalco

Department of Experimental Medicine, University of Campania

Sarah Kadzielski

Department of Pediatrics, Harvard Medical School

Geraldine Leader

Irish Center for Autism and Neurodevelopmental Research (ICAN), Department of Psychology, National University of Ireland Galway

Emmanuelle Le Chatelier

INRA https://orcid.org/0000-0002-2724-0536

Alessio Fasano

Massachusetts General Hospital https://orcid.org/0000-0002-2134-0261

Biological Sciences - Article

Keywords:

Posted Date: November 10th, 2026

DOI: https://doi.org/10.21203/rs.3.rs-11666092/v1

License: This work is licensed under a Creative Commons Attribution 4.0 International License. Read Full License

Additional Declarations: Yes there is potential Competing Interest. E.L., B.T. and S.O.F. are inventors in a patent application protecting the use of OT-mimetic bacterial proteins (FR2507542, PCT/EP2026/069928). Other co-authors declare no conflict of interest concerning this study.

Article

Ligilactobacillus salivarius enolase is an oxytocin-like systemic signal and it is reduced in children with autism spectrum disorder

Emilie Lahaye[1#], Benjamin Thomas[1#], Marion Nicol[1], Alizée Lanon[2], Philippe Chan[3], Lisa Wallart[1], Ilaria Olivito[1], Amaël Robert[1], Karthi Duraisamy[1], Benjamin Lefranc[1], Jérôme Leprince[1], Arnaud Arabo[4], Dario Siniscalco[5,6], Sarah Kadzielski[7], Geraldine Leader[8], Emmanuelle Le-Chatelier[2], Alessio Fasano[6,7], GEMMA consortium[$] and Sergueï O. Fetissov[1]*

[1]Neuroendocrine, Endocrine and Germinal Differentiation and Communication Laboratory, Inserm UMR1239, University of Rouen Normandie, Rouen, France;

[2]MetaGenoPolis, INRAE, Jouy-en-Josas, France;

[3]HeRacLeS, INSERM US51, CNRS UAR 2026, University of Rouen Normandie, Institute for Research and Innovation in Biomedicine (IRIB), Rouen, France;

[4]Biological Resources Service, University of Rouen Normandie, INSERM US51, CNRS UAR 2026, HeRacLeS, Institute for Research and Innovation in Biomedicine (IRIB), Rouen, France;

[5]Department of Experimental Medicine, University of Campania, Naples, Italy;

[6]European Biomedical Research Institute of Salerno (EBRIS), Salerno, Italy;

[7]Department of Pediatrics, Harvard Medical School, Boston, MA, USA;

[8]Irish Center for Autism and Neurodevelopmental Research (ICAN), Department of Psychology, National University of Ireland Galway, University Road, Galway, Ireland.

Short Title: ***L. salivarius* enolase is an oxytocin-like systemic signal**

Manuscript contains: 6318 words, 5 figures, 2 tables, 72 bibliographic references
Extended Data includes: 12 figures

[#]Authors who contributed equally to this study

[$]For the authors' list of "Genome, Environment, Microbiome & Metabolome in Autism", GEMMA consortium, see supplementary data.

*Corresponding author: Prof. Sergueï O. Fetissov, Tel: +332 35 14 61 93
E-mail: Serguei.Fetissov@univ-rouen.fr

Summary

Oxytocin (OT) is a peptide hormone promoting social interactions and reducing anxiety, both core behaviors altered in autism spectrum disorder (ASD)[1]. Current approaches to boost OT signaling in the brain have, however, had little success[2]. OT is carried in the blood by immunoglobulin G (IgG), suggesting a new therapeutic target for boosting OT, but its antigenic origin and capacity to influence central OT signaling are unknown[3]. Here we show that *Ligilactobacillus salivarius* (*LS*) 48 kDa enolase (ENO) displays a species-unique structural homology with OT underlying both its OT-like antigenic and ligand properties. While *LS* ENO was naturally present in human plasma, correlating between members of the same family, its levels were reduced in children of both sexes diagnosed with ASD, starting from the disorder's onset. Using mice, we show that *LS* ENO was present in both plasma and brain, and that its levels were lower in BTBR mice, a model of ASD. We further show that *LS* ENO immunization induced OT-binding IgG, which enhanced OT stability in plasma, increased OT receptor activation, and facilitated OT entry into the brain. Accordingly, *LS* ENO-immunization boosted OT concentrations in the brain and improved social, repetitive and anxiety-like behavior in BTBR mice. Thus, *LS* ENO is an OT-like protein which enhances OT signaling and boosts brain OT levels via production of OT-carrier IgG. Reduced plasma levels of *LS* ENO may, hence, contribute to ASD pathophysiology.

Keywords

oxytocin; oxytocin receptor; oxytocin carrier; enolase; lactic bacteria; immunoglobulin; gut microbiota-brain axis; hypothalamus; autism; animal models.

Main

Oxytocin (OT) is a nine-amino-acid peptide hormone produced mainly in the hypothalamus and secreted into the blood and the brain, regulating multiple physiological functions and behaviors, particularly in connection with reproduction and social behavior [4,5]. OT displays anti-stress, anxiolytic, and anorexigenic effects; it facilitates social interactions and reduces aggression [6,7], and is involved in neonatal brain development [8-10]. Deficient central OT may play a key role in the pathophysiology of autism spectrum disorder (ASD), justifying the OT system as a therapeutic target [11-13]. Nevertheless, attempts to boost OT in the brain of patients with ASD, *e.g.,* by its intranasal delivery, did not yield sustained therapeutic effects [14-17]. These data highlight the complexity of influencing OT signaling, indicating that new biotherapeutic approaches are needed [18].

It was recently demonstrated that the majority of OT in the blood is bound to immunoglobulin G (IgG), playing a role of a carrier protein. Such OT-binding IgG modulates activation of the OT receptor (OT-R), underlying individual variability in OT-mediated signaling [3]. Improving the IgG OT carrier function may represent a new alternative strategy for enhancing central OT signaling. However, the antigenic origin of OT-binding IgG and its impact on the brain OT levels are unknown.

We hypothesized that OT-binding IgG antibodies are normally produced in response to specific protein-antigens from commensal microorganisms according to the concept of molecular mimicry [19]. Our search was focused on *Lactobacilli* and *Bifidobacteria*, lactic bacteria being the first major inhabitants of the infant gut [20,21]. In this context, gut microbiota appeared recently as an important factor in the regulation of brain function and behavior relevant to ASD [22-24]. Notably, lactic bacteria, used as probiotics, have positive health effects in patients with ASD [25]. These bacteria could well act via the host OT system, since a prosocial effect of *Limosilactobacillus reuteri* (*LR*) was abolished in mice with deficient central OT-R signaling [26].

Here, an OT-like targeted proteomic approach was applied to *Ligilactobacillus salivarius (LS)*, selected upon initial screening of several species of lactic bacteria for the presence of OT-like immunoreactivity. We report the identification of *LS* enolase (ENO) as an OT-like protein displaying a unique structural homology with OT. We show that *LS* ENO has the properties of both an OT-like antigen, and a weak OT-like ligand activating human OT-R. *LS* ENO was present in systemic circulation of both humans and mice and was also detected in the mouse brain. Importantly, using the clinical cohort of the GEMMA study, we found that plasma levels of *LS* ENO were reduced in children diagnosed with ASD. The OT-like antigenic properties of *LS* ENO to produce OT-binding IgG were confirmed by immunization of mice, including BTBR mice, a model of ASD. We show that *LS* ENO-induced IgG displays a superior OT carrier function, increasing OT delivery to the brain, protecting OT from degradation in plasma, and enhancing OT-R activation. As a consequence, *LS* ENO immunization boosted OT levels in the brain and improved social, repetitive and anxious behavior in BTBR mice. Collectively, these data suggest that *LS* ENO has therapeutic value for ASD protection via enhancing OT signaling, as well as a potential ASD biomarker.

Identification of oxytocin-like proteins in lactic bacteria by targeted proteomics

To detect the presence of OT-like cross-reactivity, we analyzed, using OT ELISA, protein extracts from several lactic bacteria, including five *Lactobacilli* and five *Bifidobacteria* species. Reactivity was compared with endogenous OT levels in mice (Fig. 1a and Table 1). We found that all tested lactic bacteria displayed OT-like cross-reactivity comparable to OT levels in the mouse hypothalamus, and notably pronounced levels detected in *LS, Lacticaseibacillus camelliae* (*LC*), and *Bifidobacterium ruminantium* (*BR*) (Fig. 1a). In contrast, OT-like reactivity was low in *Escherichia coli (E. coli)* and *Hafnia alvei (H. alvei)*. The presence of OT-like cross-reactivity in protein extracts of lactic bacteria was then studied using 2-dimensional gel electrophoresis (2DGE) and immunodetection by polyclonal OT antibodies. We found that all tested bacteria displayed OT-like positive protein spots which were stronger in *Lactobacilli*, with *LS, Lactobacillus gasseri* (*LG*), *Lactiplantibacillus plantarum* (*LP*) and *LR* displaying a distinct OT-like signal around 50 kDa, which was particularly strong in *LS* (Fig. 1c and Extended [Ext.] Data Fig. S1). Based on both ELISA and 2DGE results, as well as previous data showing anti-stress probiotic effects of *LS* [27,28], this bacterial species was selected for the further identification and functional validation of OT-like proteins.

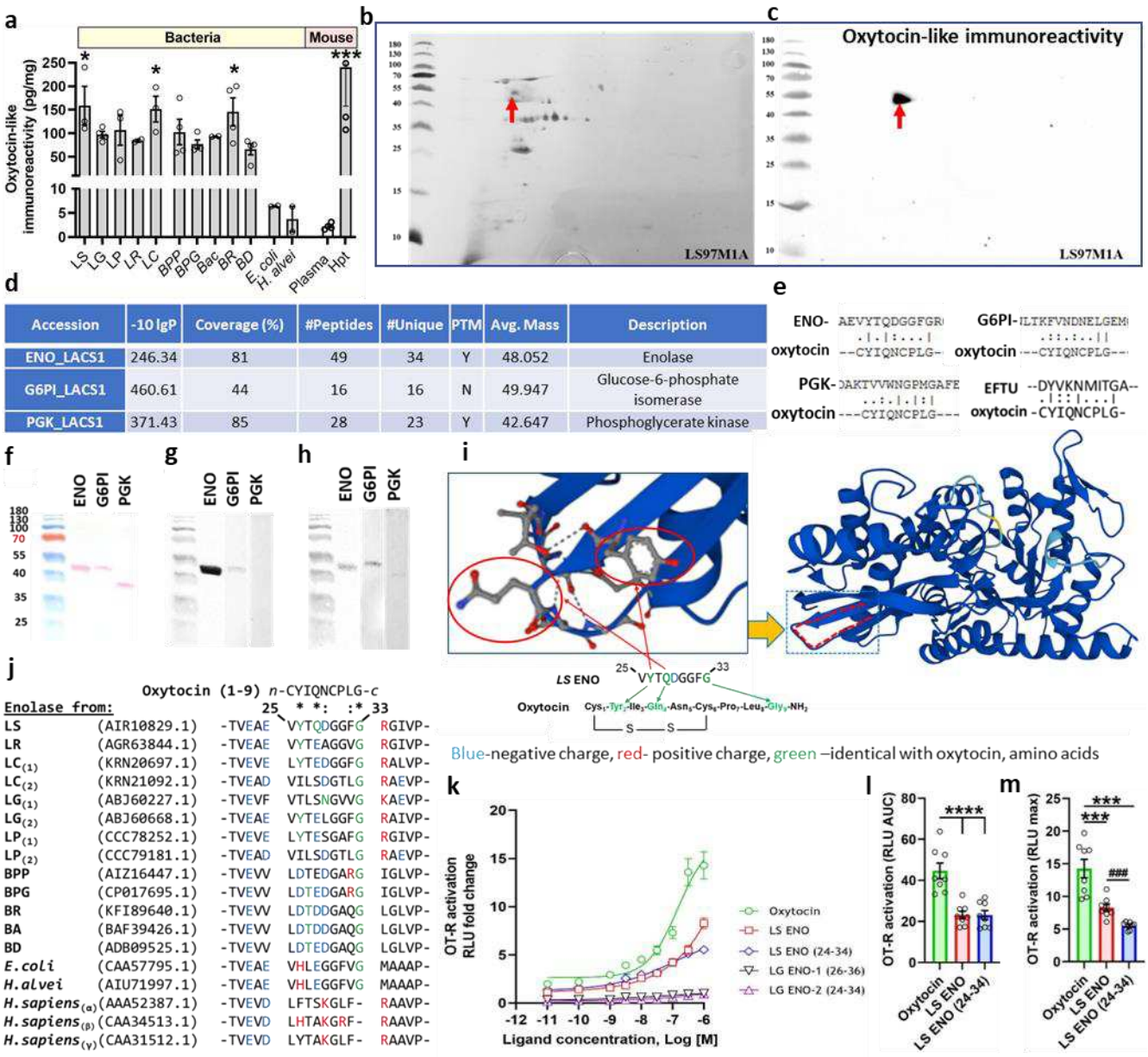


Fig. 1. Proteomic identification of OT-like bacterial proteins. a. Screening for OT-like immunoreactivity in bacterial species by ELISA. Tested *Lactobacilli*: *Ligilactobacillus salivarius* (*LS*), *Lactobacillus gasseri* (*LG*), *Lactiplantibacillus plantarum* (*LP*), *Limosilactobacillus reuteri* (*LR*) and *Lacticaseibacillus camelliae* (*LC*). Tested *Bifidobacterium* (*B*) species: *B. pseudolongum* subsp. *pseudolongum* (*BPP*), *B. pseudolongum* subsp. *globosum* (*BPG*), *B. adolescentis* (*Bac*), *B. ruminantium* (*BR*), and *B. dentium* (*BD*). Tested *Enterobacteria*: *Escherichia coli (E. coli)* and *Hafnia alvei* (*H. alvei*). Tested mouse tissues: hypothalamus (Hpt) and plasma. **b**. 2DGE of the membrane protein fraction of *LS* grown in aerobic conditions, followed by immunodetection with polyclonal OT IgG (**c**). Red arrows point to the OT-like positive spot (**c**) and the corresponding protein spot in the silver staining gel used for protein identification (**b**). **d**. Mass spectrometry identification of OT-like protein candidates from (**b**). **e**. Amino acid sequence homology between OT and three OT-like protein candidates, enolase (ENO), glucose-6-phosphate isomerase (G6PI) and phosphoglycerate kinase (PGK) identified in aerobic conditions as well as elongation factor Tu (EFTU) identified in anaerobiosis. **f**. Polyacrylamide gel electrophoresis of recombinant *LS* ENO, G6PI and PGK proteins, stained with Ponceau red. **g**. OT Western blot. **h**. OT Western blot after pre-absorption of OT antibody with OT (10^{-6} M). **i**. OT-like motif of LS ENO (25-33) is located in the β-sheet on the surface of the protein, exposing the tyrosine, Tyr (Y), and glutamine, Gln (Q) residues, UniProt (Q1WSY0). **j**. Sequence alignment between OT and

ENO from *LS* and from other tested bacterial species, as well as from human ENO, annotated with GenBank references. **k**. Activation of OT-R in vitro using β-arrestin recruitment assay in relative luminescence units (RLU), tested by OT, full-size 48 kDa *LS* ENO, OT-like *LS* ENO (24-34) fragment, and fragments from two ENO isoforms of *LG*, *LG* ENO-1 (26-36) and *LG* ENO-2 (24-34), n=8, in triplicate. **l**. Area under the curve (AUC) and **m.** Maximal (max) OT-R activation. **a**, ANOVA, *p<0.05, ***p<0.001, Dunnett's multiple comparisons test *vs.* plasma.

Total *LS* protein was extracted in the stationary phase after 24h of growth in the planktonic cultures, which were similar between aerobic and anaerobic conditions. However, *LS* colonies grown in agar were larger in anaerobiosis, justifying this species as an aerotolerant anaerobe (Ext. Data Fig. S2a,b). To determine the subcellular localization of OT-like proteins, *LS* protein extract was fractionated by ultracentrifugation and analyzed by Western blot with anti-OT antibodies. OT-like immunoreactive bands were present in both aerobic and anaerobic growth conditions, with the strongest band of about 50 kDa, which was most distinct in the membrane fraction in aerobiosis (Ext. Data Fig. S2c,d). This condition was then privileged for further identification of OT-like proteins by 2DGE and immunodetection with OT antibodies (Fig. 1b,c). Using this technique, a single, about 50 kDa OT-like positive spot was detected (Fig. 1c), and the corresponding spot in the gel was dissected for protein identification (Fig. 1b). As behind each gel spot there could be several proteins with a similar molecular weight, it is not surprising that mass spectrometry analysis revealed several proteins located at the OT-like positive spot. Among them, ~48 kDa enolase (ENO) had the highest score considering both the percentage of sequence coverage and the number of peptides found (Fig. 1d). Two other proteins, ~50 kDa glucose-6-phosphate isomerase (G6PI) and ~43 kDa phosphoglycerate kinase (PGK) were also well represented (Fig. 1d). ENO was also detected in OT-like spots of both the soluble and residual *LS* protein fractions in anaerobic and anaerobic conditions (Ext. Data Fig. S2e-h and S3). In the latter, in addition to the three proteins reported above, ~44 kDa elongation factor Tu (EFTU) was also identified (Ext. Data Fig. S4a-c). The amino acid sequences of the *LS* ENO, G6PI, PGK and EFTU were aligned with human OT, showing discontinuous sequence homology present in all four bacterial proteins potentially qualifying them as OT-like targets via conformational mimicry (Fig. 1e).

Recombinant *LS* proteins ENO, G6PI and PGK were synthesized, displaying a single band of expected molecular weight for each protein (Fig. 1f). However, Western blot revealed the presence of potent OT-like immunoreactivity only in ENO (Fig. 1g). Pre-absorption of OT antibody with synthetic OT peptide, as a specificity control, abolished the ENO protein immunostaining, but did not change the weak staining of G6PI, confirming the presence of OT-like structural homology only within the ENO protein (Fig. 1h). Western blot of *Pseudomonas aeruginosa* EFTU, which has an identical OT-like motif and was available in the laboratory, did not show OT-like cross-reactivity (Ext. Data Fig. S3). These results justified the selection of *LS* ENO for functional validation as an OT-like protein.

The structural homology between *LS* ENO and OT was further analyzed. Although the OT-like *LS* ENO (25-33) motif contained only three amino acids identical with OT, *i.e.* tyrosine (Tyr, Y), glutamine (Gln, Q) and glycine (Gly, G), both Tyr and Gln were located at the tip of a β-sheet, *i.e.* accessible for OT antibody binding mimicking the corresponding amino acids exposed by the OT ring (Fig. 1i). We also found that the OT-like *LS* ENO (24-34) fragment was specific to *LS*; it was absent in ENO of other tested bacterial species and in its human homologues (Fig. 1j). Moreover, sequence alignment of 283 ENO from *Lactobacillaceae* confirmed that the OT-like motif of *LS* is a unique feature of this species (Ext. Data, Fig. S5).

LS ENO activates oxytocin receptor

To validate the presence of the OT-like motif in *LS* ENO, we tested whether it may act as a direct OT-like ligand, using β-arrestin recruitment assay in HTLA cells expressing human OT-R. An OT-like *LS* ENO (24-34) peptide fragment was synthesized, flanked by oppositely charged amino acids glutamate (E) and arginine (R) to ensure the β-sheet formation (Fig. 1j). As a negative control of random peptides sharing several amino acids with *LS* ENO (24-34), two *LG* ENO isoforms fragments, *LG* ENO-1 (26-36) and *LG* ENO-2 (24-34), both missing the "Tyr - Gln"

pair in the sequence (Fig. 1j), were synthesized. Human synthetic OT was used as a positive control, showing expected dose-dependent OT-R activation (Fig. 1k). We found that both the full-size 48 kDa *LS* ENO and its OT-like *LS* ENO (24-34) fragment activated the OT-R with a similar potency (Fig. 1k,l). However, the maximal activation was higher for the full protein (Fig. 1m). The OT-R activation by *LS* ENO was about two times less potent than that induced by OT at similar molar ratios, still, the activation started from nanomolar concentrations (Fig. 1k). Any of *LG* ENO fragments did not affect OT-R activation, pointing to the specific OT-like feature of the *LS* ENO fragment (Fig. 1k). Thus, these results validated *LS* ENO as a protein containing an OT-like motif able to weakly activate OT-R, a molecular mimicry apparently specific to ENO of the *LS* species.

LS ENO is present in human plasma and reduced in children with ASD

Next, the relevance of *LS* ENO to ASD in humans was studied by analyzing its plasma levels in the prospective cohort of the GEMMA project [29]. For this purpose, we developed an *LS* ENO ELISA, which lacks cross-reactivity with OT, but may weakly react with ENO from some other *Lactobacillus* species (Ext. Data, Fig. S6). Plasma samples were taken from infants (ranging from 4- to 60-months-old) with and without an ASD diagnosis. In total, 52 infants diagnosed with ASD based on the Brief Observation of Symptoms of Autism (BOSA) scale, including 28 boys and 24 girls, and 39 healthy infants, including 20 boys and 19 girls, as well as their families, including mother, father, and a healthy sibling, were analyzed. Study subjects were recruited by three centers in Ireland, Italy, and the USA. Infants were analyzed at different ages, including 15 boys and 15 girls who had an initially negative BOSA score (BOSA-), but later became BOSA positive (BOSA+). Several Controls' but only a few ASD families were recruited by the US and Italian centers (Ext. Data Fig. S7). We found that *LS* ENO signal was present in plasma at variable levels in all studied subjects without significant sex differences.

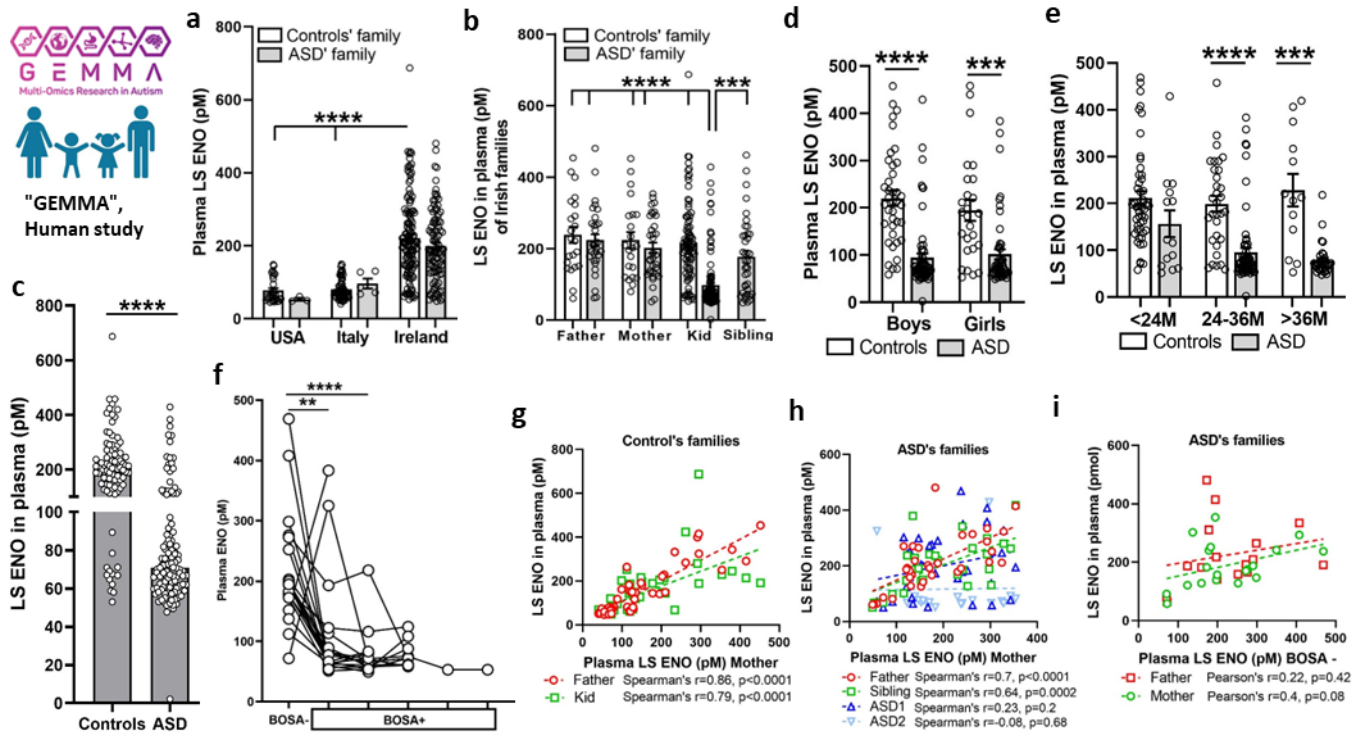


Fig. 2. Detection of *LS* ENO in human plasma from the GEMMA study. a. *LS* ENO in Controls' and ASD's families (without ASD cases) from 3 recruitment centers. **b-i**. *LS* ENO data only from the Irish cohort. **b**. *LS* ENO in family members. **c**. *LS* ENO in healthy (Controls) and ASD children for all ages and sexes combined and, for two sexes separately (**d**), as well as for different ages in months (M) in both sexes (**e**). **f.** Plasma *LS* ENO dynamics measured at different intervals in the same children who were initially ASD negative (BOSA-) but became ASD positive (BOSA+). *LS* ENO correlations between family members in Control's (**g**) and ASD's (**h**) families. **i**. *LS* ENO

correlations between BOSA- children before they became BOSA+ and their parents. BOSA, brief observation of symptoms of autism. **a,b,d,i,** K.W, Dunn's post-tests **p<0.01, ***p<0.001, ****p<0.0001. **c,** Mann-Whitney tests, ****p<0.0001. **f**. Paired t-tests, **p<0.01, ****p<0.0001, **g-i**, Spearman's and Pearson's 2-tailed correlation tests.

Comparison of families from the three recruitment centers, excluding ASD cases, showed that *LS* ENO plasma levels were higher in both Control and ASD families from Ireland as compared to Control families from both the USA and Italy (Fig. 2a). Because of such prominent geographical differences, only the Irish cohort was further used to compare *LS* ENO between ASD cases and Controls. Within this cohort, kids diagnosed with ASD displayed strongly reduced *LS* ENO plasma concentrations as compared to all their family members (Fig. 2b). Remarkably, *LS* ENO median values in ASD cases were nearly three times lower than in Control kids (70.9 pM *vs.* 205.1 pM, respectively, Fig. 2c). ASD-associated reduction of *LS* ENO was present in both boys and girls (Fig. 2d) and it was significant starting from 24-months of age (Fig. 2e). Moreover, in kids diagnosed with ASD, but who had initial negative BOSA, a significant decrease of *LS* ENO plasma concentration was observed when BOSA become positive (Fig. 2f). To test for the possible family influence on *LS* ENO plasma levels, we analyzed correlations between family members. In Control families, mother's *LS* ENO correlated positively with *LS* ENO in both father and kid (Fig. 2g). In ASD families, such correlation was also present between the mother and both father and healthy sibling, but it was lost for ASD kid as assayed at the first (ASD1) and a later (ASD2) blood sampling associated with BOSA+ (Fig. 2h). However, in ASD kids who had initial BOSA negative status, during this status, plasma *LS* ENO level was still weakly associated with that of the mother (Fig. 2i). Thus, *LS* ENO was identified as an OT-like systemic signal present in healthy humans, while its reduced plasma level was linked to ASD, starting from the disorder onset. The mechanistic relevance of *LS* ENO to ASD, focusing on its possible role as an OT-like antigen inducing OT-carrier IgG, which can modulate host OT signaling and ASD-like behavior, was then studied in mice.

LS ENO immunization of C57Bl6 mice induces oxytocin-binding IgG reaching the brain

The potential of *LS* ENO to induce OT-binding IgG was tested by active immunization. For this purpose, in a first approach (Exp #1, Ext. Data Fig. S8a), healthy C57Bl6 male mice received by intraperitoneal (IP) injection 50 μg of the full-size *LS* ENO protein or *LS* ENO (24-34) peptide in complete Freund's adjuvant (CFA) followed by a boost after two weeks of either molecule in incomplete Freund's adjuvant (IFA). A control group received 0.9% NaCl solution (NaCl). Moreover, as a control for a non-specific immunomodulatory effect of CFA and IFA, one group of mice received adjuvants (Adj) only. Efficiency of *LS* ENO immunization, 21 days after the first injection, was confirmed by increased plasma *LS* ENO-reactive IgG levels (Fig. 3a). In contrast, mice immunized with the *LS* ENO (24-34) fragment had similar levels of *LS* ENO IgG with the group receiving Adj only (Fig. 3a). Importantly, mice immunized with *LS* ENO developed elevated plasma levels of OT-binding IgG (Fig. 3b). A weaker response was induced in *LS* ENO (24-34)-immunized group (Fig. 3c), suggesting that this fragment's flanking regions are necessary for a stronger OT-binding IgG response, in agreement with molecular mimicry concept [19].

Subsequently, a new series of healthy C57Bl6 male mice (Exp #2, Ext. Data Fig. S8b) was immunized with *LS* ENO. OT-like antigenic effect of *LS* total protein extract was also analyzed. The efficiency of *LS* ENO immunization was confirmed by an elevated titer of *LS* ENO-reactive IgG, while a weaker response was induced by *LS* total protein (Fig. 3d). Before the immunization, OT-reactive IgG was present in all mice without significant group differences (K.-W.-test, p=0.69). Mice immunized with *LS* ENO developed higher levels of OT-binding IgG (Fig. 3e). The OT-like IgG response to the *LS* protein extract was weaker, suggesting that the ENO protein was solely responsible for the OT-like cross-reactivity (Fig. 3e,f). Thus, together with Exp #1, these results validated *LS* ENO as an antigen mimetic of OT, stimulating development of OT-binding IgG in healthy mice.

To substantiate our hypothesis that OT-binding IgG may transport OT to the brain, OT-binding IgG was also measured in mouse brain tissue. For this purpose, we used ELISA with either normal or dissociative buffer conditions, allowing the detection of free and total OT-binding IgG, respectively, the latter due to dissociation of

immune complexes (IC). OT-binding IgG antibodies were detected in the hypothalamus, likely due to the fenestrated blood vessels in the hypothalamic median eminence, but not in any other tested brain regions, including the amygdala and prefrontal cortex (PFC). While no significant group differences were found for OT-binding free IgG (Fig. 3g), their total levels were increased in *LS* ENO-immunized mice (Fig. 3h), indicating an increased percentage of IgG present in IC (Fig. 3i). Aligned with this finding, increased binding affinity of IgG for OT (lower K_D), measured by surface plasmon resonance (SPR), was present in *LS* ENO-immunized mice (Fig. 3j). Such increased affinity was mainly due to an increased association rate (k_a,) while the dissociation rate (k_d) was unchanged (Fig 3k,l). The changes of IgG binding properties for OT are thus modified by *LS* ENO immunization (Fig. 3m).

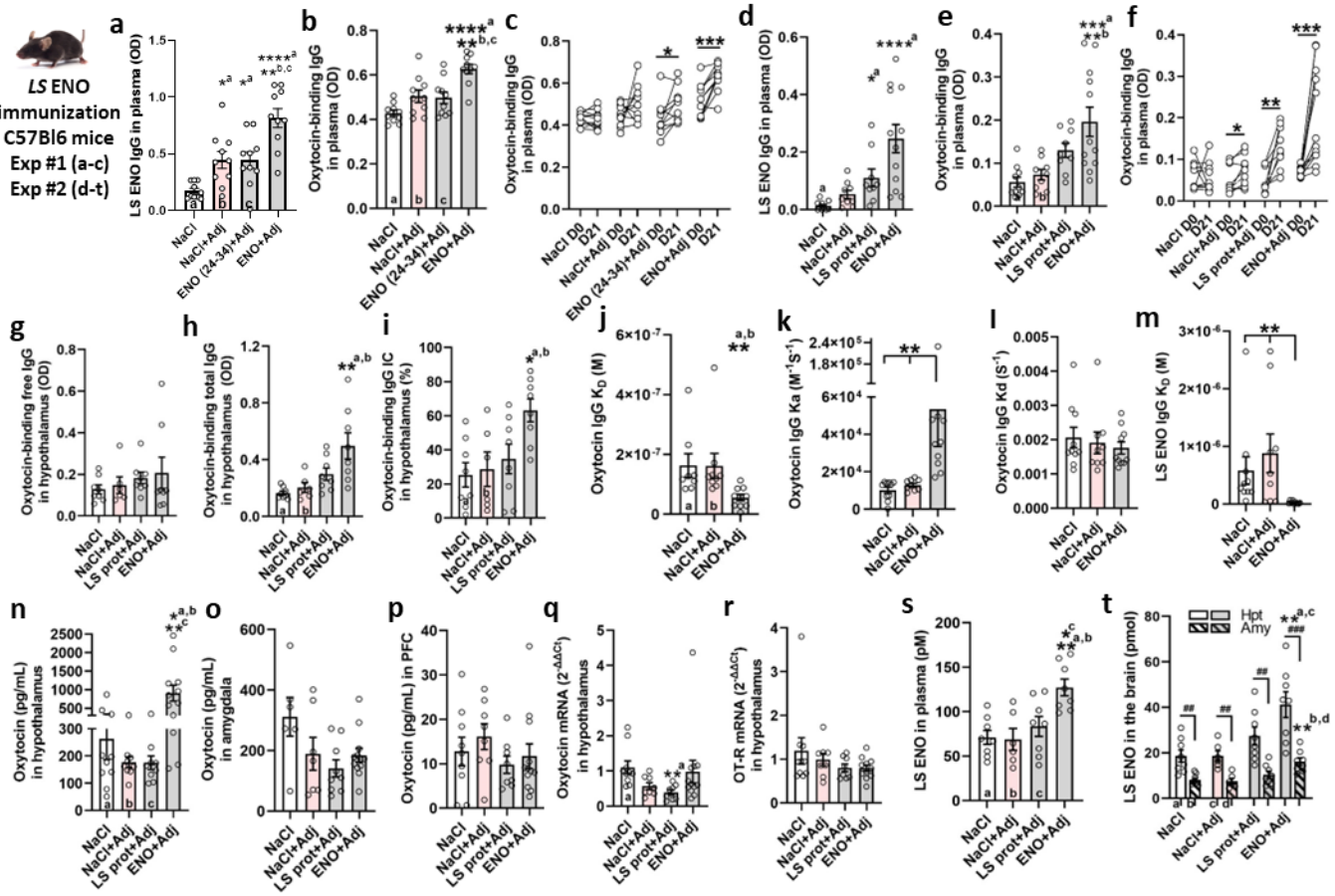


Fig. 3. Functional validation of *LS* ENO as an OT-like antigenic protein in healthy mice. **a-c.** Exp #1 in C57Bl6 mice receiving saline only (NaCl) as a non-treated control or saline with adjuvant (NaCl+Adj) as a control for non-specific immunization, or immunized with OT-like *LS* ENO fragment ENO (24-34)+Adj or with *LS* ENO (ENO+Adj). **a**. Plasma levels of ENO-binding IgG in optical density (OD) at 405 nm. **b**. Plasma levels of OT-binding IgG. **c**. Dynamics of plasma levels of OT-binding IgG from Day 0 (D0) to D21 after immunization. **d-t**. Exp #2 in C57Bl6 mice receiving saline only (NaCl) or saline with adjuvant (NaCl+Adj) or immunized with *LS* total protein extract (*LS* prot+Adj) or with *LS* ENO (ENO+Adj). **d**. Plasma levels of *LS* ENO IgG. **e**. Plasma levels of OT-binding IgG. **f**. Dynamics of OT-binding IgG in plasma from D0 to D21 after immunization. **g-i.** OT-binding IgG in the hypothalamus assayed as free (**g**), total (**h**), and immune complexes (IC,**i**). **j-l.** Affinity kinetics of IgG binding to OT, including dissociation at equilibrium constant (K_D) in moles (M) in (**j**), as well as association k_a (**k**) and dissociation k_d (**l**) constants. **m.** Affinity of IgG for *LS* ENO. **n-p**. Levels of OT peptide in the brain including the hypothalamus (**n**), amygdala (**o**), and prefrontal cortex (PFC, **p**). Levels of OT mRNA (**q**) and OT-R mRNA (**r**) in the hypothalamus. **s**. *LS* ENO levels in plasma. **t**. *LS* ENO levels in the hypothalamus (Hpt) and amygdala (Amy). **a,b,d,e,h,i,n,q,s,t,** ANOVA, Tukey's post-

tests, *p<0.05, **p<0.01, ***p<0.001, ****p<0.0001, **c, f**, Paired t-test *p<0.05, **p<0.01, ***p<0.001. **j**,**k**,**m,** Kruskal-Wallis (K.-W.) test, Dunn's post-test, **p<0.01. **t**, Student's t-test, ##p<0.01, ###p<0.001.

LS ENO immunization of C57Bl6 mice boosts oxytocin and *LS* ENO levels in the brain

Effect of *LS* ENO immunization on OT levels in the brain in Exp #2 was analyzed by ELISA in mouse brain tissue homogenates. We found that in the hypothalamus of *LS* ENO-immunized mice, OT concentrations were higher than in other study groups (Fig. 3n). No significant differences in OT peptide were present in the amygdala and PFC (Fig. 3o,p). Increased hypothalamic OT levels were not accompanied by significant changes in OT mRNA expression (Fig. 3q). OT-R mRNA levels were not significantly affected (Fig. 3r). Thus, *LS* ENO immunization boosted OT levels in the hypothalamus of healthy mice independently of its local gene expression.

To determine if *LS* ENO is present in mouse plasma and brain tissue we used the same *LS* ENO ELISA as for the human studies. *LS* ENO was detected in plasma of all studied C57Bl6 mice at mean concentrations ~70 pM in non-immunized controls. At the same time, *LS* ENO immunization almost doubled *LS ENO* plasma levels (Fig. 3s). In the brain, *LS* ENO was measured in the same tissue homogenates used for the OT assay. We found that *LS* ENO was present at about 19 and 8 pmol in the hypothalamus and amygdala, respectively, of non-treated C57Bl6 mice (Fig. 3t), while it was not detectable in the PFC. Remarkably, *LS* ENO immunization doubled its concentrations in both brain regions (Fig. 3t). As a negative control, the presence of *LS* ENO was studied in germ-free mice. It was not detectable either in plasma or in the brain (data not shown), confirming the microbial origin of the signal detected in the hypothalamus and amygdala of conventional mice. These results show that in the mouse, *LS* ENO is a bacteria-derived signal which may act both systemically and in the brain, and further suggest a facilitating role of IgG in transporting *LS* ENO and OT to the brain.

LS ENO immunization induces oxytocin-binding IgG in BTBR mice

Following the demonstration of *LS* ENO OT-like antigen-mimetic properties in healthy mice, *i.e.,* its ability to induce OT-binding IgG boosting both OT and *LS* ENO levels in the brain, in Exp #3, we studied if *LS* ENO immunization may alleviate ASD-like symptoms in BTBR mice, a mouse strain commonly used as a model of idiopathic ASD [30] (Ext. Data, Fig. S8c). As a control for *LS* ENO OT-like antigenic property, one group of BTBR mice was immunized with synthetic human OT, and another group was a control for a non-specific adjuvant effect. One week after the boost, mice underwent behavioral testing as presented below, and then, 35 days after the first immunization (D35), plasma and brain tissues were analyzed. *LS* ENO-immunized BTBR mice developed high plasma *LS* ENO IgG levels (Fig. 4a), reflecting a strong adaptive immune response, even though alteration of such response was previously reported in this strain of mice [31]. As expected, *LS* ENO immunization induced OT-binding IgG (Fig. 4b), but no such response was observed in OT-immunized mice, *i.e.* showing that OT itself is a weak immunogen. OT-binding IgG was also detected in the hypothalamus, but not in the amygdala and PFC. Notably, while hypothalamic levels of OT-binding free IgG were not different among the study groups (Fig. 4c), OT-binding total IgG was higher in *LS* ENO-immunized mice (Fig. 4d), indicating an increase of IgG present in IC (Fig. 4e). Of interest, the basal levels of total OT-binding IgG, but not the percentage of IC (data not shown), were higher in the hypothalamus of BTBR *vs.* C57Bl6 mice (Fig. 4f). These results agree with previously reported increased plasma IgG levels in BTBR mice [32]. Then, IgG was extracted from plasma and analyzed for OT binding affinity kinetics using SPR. We found that *LS* ENO-immunized BTBR mice had IgG characterized by higher affinity for OT (Fig. 4g), *i.e.* showing a similar response to *LS* ENO immunization as C57Bl6 mice, indicating increased carrier capacity of IgG for OT. To investigate the functional consequences, we next analyzed OT levels and behavioral changes in immunized mice.

LS ENO immunization boosts oxytocin and *LS* ENO levels in plasma and the brain of BTBR mice

Plasma OT levels were increased in both OT- and *LS* ENO-immunized BTBR mice, with a stronger increase in the latter group (Fig. 4h). Indeed, increased brain tissue concentrations of OT were present only in *LS* ENO-immunized mice, including in both hypothalamus (Fig. 4i) and amygdala (Fig. 4j), without differences in the PFC (Fig. 4k). Increase of OT levels, was again not accompanied by increased local OT mRNA expression, neither in the hypothalamus nor amygdala (Fig. 4l,m). However, in the PFC, OT mRNA levels were slightly elevated (Fig. 4n). OT-R mRNA levels in all three studied brain regions were not different (Ext. Data Fig. S9). Analysis of regulatory peptides and cytokine expression showed higher levels of NPY and POMC mRNA in the hypothalamus and lower levels of TNF-α in the amygdala of *LS* ENO-immunized mice (Ext. Data Fig. S9). Thus, immunization of BTBR mice with *LS* ENO increased plasma OT and boosted OT levels in both the hypothalamus and amygdala, *i.e.* in ASD-relevant therapeutic areas. Increased OT levels in the brain was not caused by altered local OT production, but instead, result from enhanced OT carrier role of IgG to transport circulating OT into the brain.

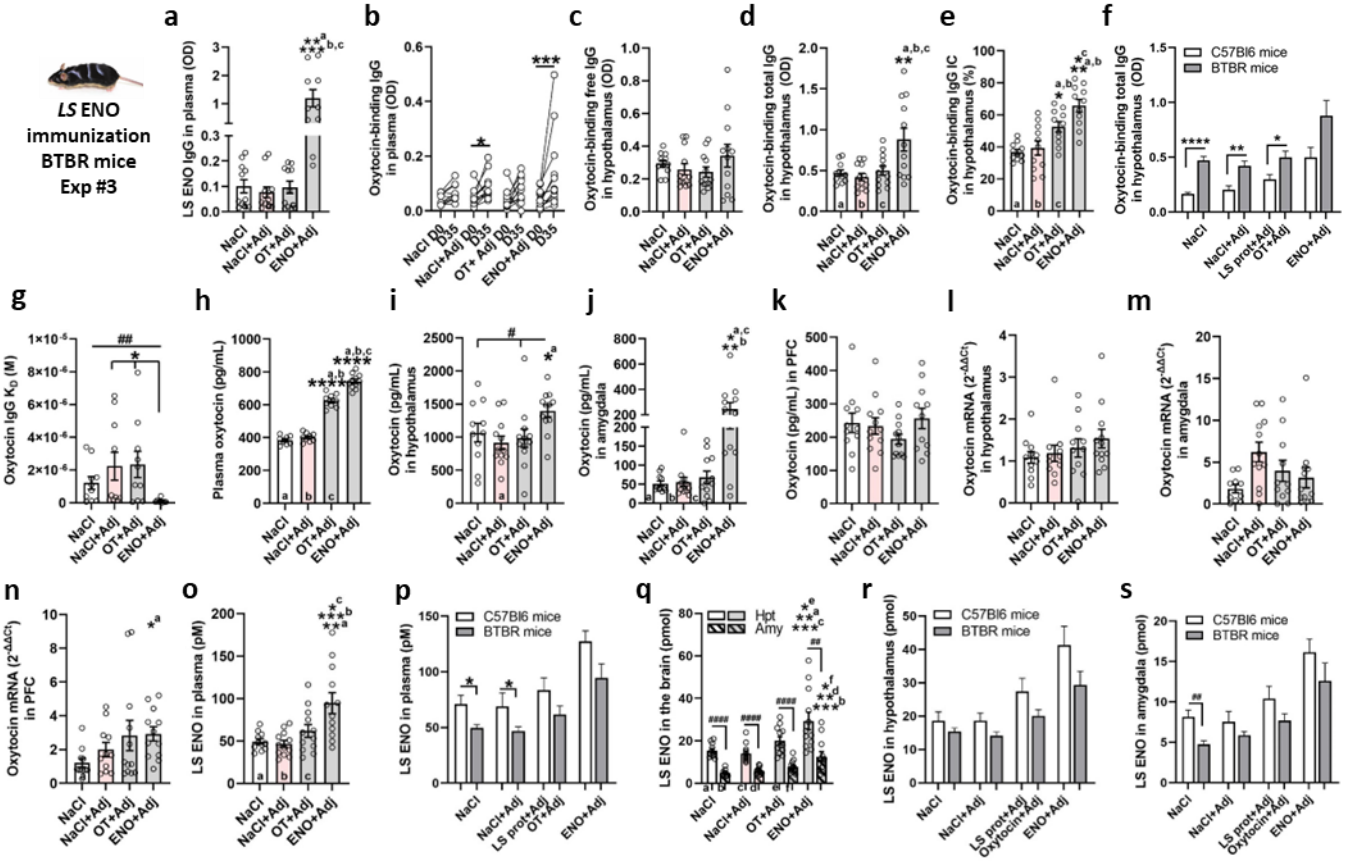


Fig. 4. **Functional validation of *LS* ENO as an OT-like antigenic protein in BTBR mice.** Analysis in four groups of female and male mice receiving saline (NaCl), saline + adjuvants (NaCl+Adj), OT+Adj, and *LS* ENO+Adj, respectively. **a**. Plasma levels of *LS* ENO IgG in optical density (OD) at 405 nm. **b**. Dynamics of plasma levels of OT-binding IgG from Day 0 (D0) to D35 after immunization. **c**-**f.** OT-binding IgG in the hypothalamus assayed as free (**c**), total (**d**), and immune complexes (IC, **e**), and as compared to C57Bl6 mice from Exp #2 (**f**). **g**. Molar (M) affinity of IgG for OT as dissociation constant at equilibrium (K_D). **h**. Plasma OT concentrations. **i-k**, OT concentrations in brain tissue, including hypothalamus (**i**), amygdala (**j**), and prefrontal cortex (PFC, **k**). OT mRNA expression in hypothalamus (**l**), amygdala (**m**), and PFC (**n**). Plasma *LS* ENO concentration in BTBR mice (**o**) and, in comparison with C57Bl6 mice from Exp #2 (**p**). **q.**-*LS* ENO levels in brain tissue of BTBR mice, including the hypothalamus (Hpt) and amygdala (Amy), and, in comparison with C57Bl6 mice for both regions, respectively (**r,s**). **a**,**d**,**e**,**h,i,j,n,o**, ANOVA, Tukey's post-tests, *p<0.05, **p<0.01, ***p<0.001, ****p<0.0001. **b**, Wilcoxon paired test *p<0.05, ***p<0.001. **g,** K.-W. test, Dunn's post-test, *p<0.05. **f,p**,

Student's t-test *p<0.05, **p<0.01, ***p<0.001, ****p<0.0001, **g,q,** Student's t-test ##p<0.01, ####p<0.0001., **s**, Mann-Whitney (M.-W.) test **p<0.01.

LS ENO was detected in plasma of BTBR mice at mean concentrations of ~50 pM in the control group and it was about twice as high in the *LS* ENO-immunized group (Fig. 4o). Notably, plasma *LS* ENO levels in non-treated BTBR mice were ~40% lower than in C57Bl6 mice (Fig. 4p). In the brain, *LS* ENO was present at about 15 and 5 pmol in the hypothalamus and amygdala, respectively, of non-treated BTBR mice, while *LS* ENO immunization doubled its concentrations in both brain regions (Fig. 4q). Thus, *LS* ENO levels tended to be lower in the hypothalamus and were significantly lower in the amygdala in BTBR than in C57Bl6 mice, suggesting reduced OT-like stimulation by *LS* ENO in the brain of BTBR mice (Fig. 4r,s), which could be counteracted by *LS* ENO immunization.

LS ENO immunization ameliorates ASD-like behavior in BTBR mice

The effects of *LS* ENO immunization on ASD-like behavior in BTBR mice were tested starting from one week after the *LS* ENO/IFA boost. Considering sex differences in behavior, the data were analyzed separately for males and females. We found that *LS* ENO immunization had a greater impact on behavior in males than in females. Indeed, using the three-chamber test for social interactions, we found that *LS* ENO-immunized males preferred to stay in the chamber with the stimulus mouse (Fig. 5a), where they were more immobile than in the chamber with the object (Fig. 5b), but the total immobility time was not affected (Fig. 5c). Importantly, in *LS* ENO-immunized males the sociability index was increased (Fig. 5d). Three-chamber tests in females showed that *LS* ENO immunization increased total immobility time but did not significantly affect other markers, which may signify decreased arousal with normal sociability (Ext. Data Fig. S10a-d). Thus, *LS* ENO immunization improved social behavior in males but not in females.

For the analysis of repetitive behavior, which is typically increased in ASD, a self-grooming test was applied. We found that *LS* ENO-immunized males spent less time in grooming and had a significant decrease in the number of grooming episodes (Fig. 5e,f). No significant differences in this test were observed in females (Ext. Data Fig. S10e-f). Thus, *LS* ENO immunization reduced repetitive behavior only in BTBR male mice.

Anxiety associated with open spaces was evaluated using an open-field test. In *LS* ENO-immunized males, the total distance traveled did not change (Fig. 5g), but the time spent in the center increased, and in the periphery decreased, resulting in higher center ratios (Fig. 5h-j). However, in *LS* ENO-immunized females, such ratios only showed a tendency to increase (Student's t-test p<0.05 *vs.* NaCl+ Adj) without significant differences in their components (Ext. Data Fig. S10g-j). Thus, *LS* ENO immunization had anxiolytic effects in BTBR male mice, but less pronounced effects in females.

Fear of heights in both humans and mice is a natural feeling, which in some subjects may lead to increased anxiety, called acrophobia. Having no fear of heights is another extreme condition, previously reported in BTBR mice and in an ASD rodent model induced by valproic acid [33,34]. The effect of *LS* ENO immunization of BTBR mice on height-associated anxiety was studied using an elevated plus-maze. We found that *LS* ENO-immunized males had a reduction in total distance traveled (Fig. 5k), increased time spent in closed arms (Fig. 5l), and a prominent decrease in time spent in open arms (Fig. 5m). Notably, in contrast to the open arms, these mice did not show a decrease in time spent in the center area, which is considered anxiogenic (Fig. 5n). In *LS* ENO-immunized BTBR females, total distance traveled was also reduced and time spent in the open arms tended to be lower (ANOVA p=0.06, M.-W. test *vs.* NaCl, p<0.05) without a decrease in time in the center area (Ext. Data Fig. S10k-n). Thus, these results demonstrate a prominent effect of *LS* ENO immunization on strengthening height-associated anxiety in males, which can be interpreted as better risk assessment. These results align with the known effects of OT to reduce risky decisions in both rodents and humans [35,36]. Taken together, *LS* ENO immunization improved social, repetitive, anxiety and risky behavior in BTBR males, but did not significantly change these behaviors in females.

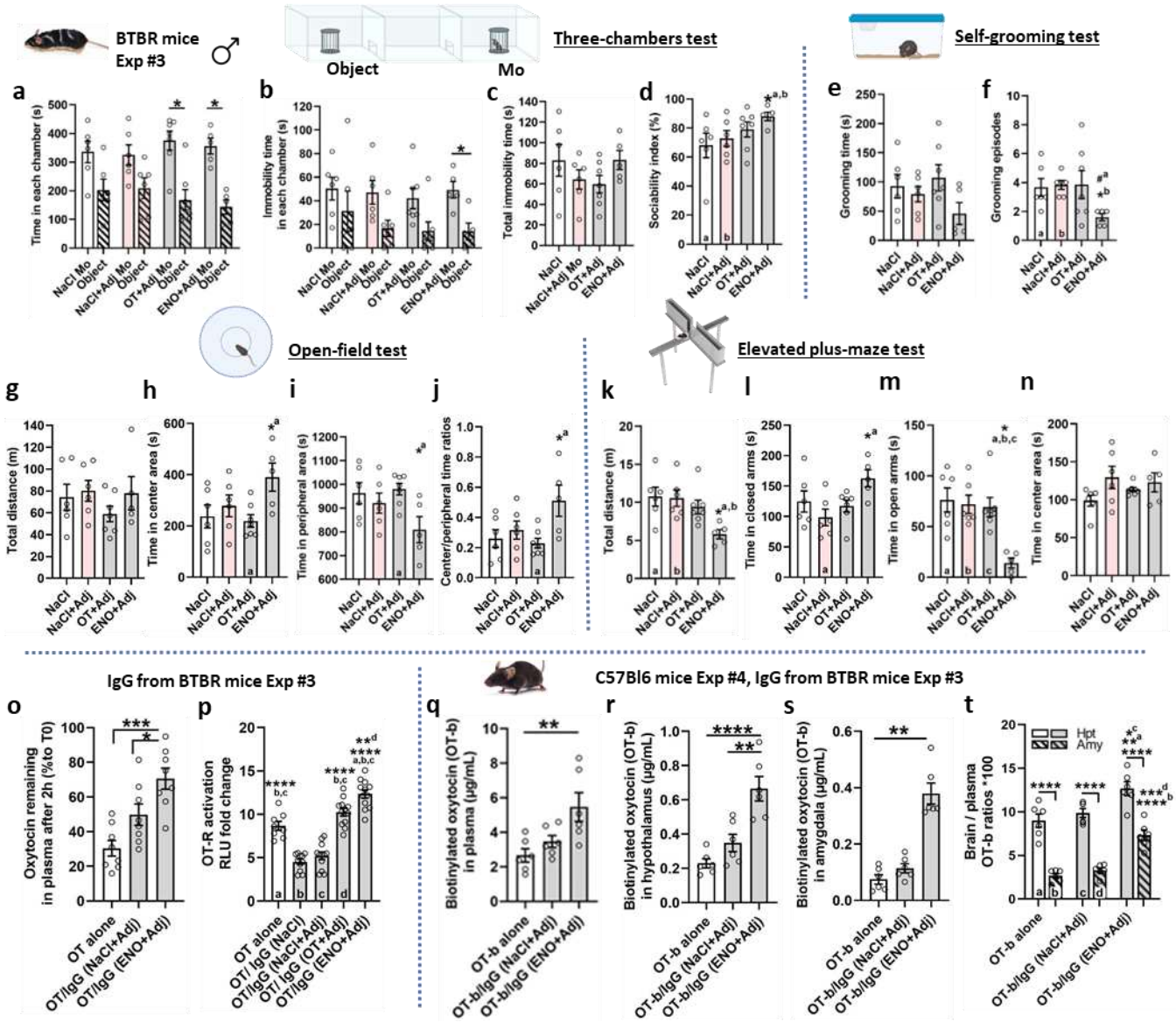


Fig. 5. Effect of *LS* ENO immunization on ASD-like behavior in BTBR mice and effects of IgG on oxytocin signaling. Analysis in four groups of male BTBR mice receiving saline (NaCl), saline + adjuvants (NaCl+Adj), OT+Adj and *LS* ENO+Adj, respectively. **a-d**. Three-chamber test including time (**a**) and immobility (**b**) in the chamber with a stimulus mouse (Mo) or with an Object. **c.** Total immobility time and **d.** sociability index. **e,f.** Self-grooming test, including grooming time (**e**) and number of grooming episodes (**f**). **g-j**. Open-field test, including total distance traveled (**g**), time spent in the center (**h**) and peripheral (**i**) areas, as well as their ratios (**j**). **k-n.** Elevated plus-maze test including total distance traveled (**k**), time spent in closed (**l**) and in open (**m**) arms and in the center area (**n**). **o**. Effect of IgG on OT stability in plasma, as a percentage of its initial level (T0, 100%) after 2h of incubation in IgG-deprived plasma, supplemented or not with IgG from two groups of BTBR mice from Exp #3. **p**. OT-R activation as measured by relative luminescence units (RLU) of β-arrestin recruitment following application of OT alone and OT with IgG from different groups of BTBR mice from Exp #3. **q-t.** Exp #4, Biotinylated OT (OT-b) concentrations in plasma (**q**), hypothalamus (**r**), and amygdala (**s**) as well as its brain/plasma ratios (**t**) in C57Bl6 mice 30 min after IP injection of OT-b alone or together with IgG BTBR mice from Exp #3. **a,b,** Paired Wilcoxon's tests *p<0.05. **d**. ANOVA p=0.1, Student's t-test *p<0.05. **f**, K-W test, p=0.02, Dunn's post-test *p<0.05, Student's t-test #p<0.05. **h-m,o-r,t**, ANOVA, Tukey's post-test *p<0.05, **p<0.01, ***p<0.001, ****p<0.0001. **s,** K-W test, Dunn's post-tests **p<0.01.

IgG protects oxytocin from degradation in plasma

As the production of OT-binding IgG leading to amelioration of ASD-like behavior in BTBR mice was associated with increased OT levels in the blood and brain, we next studied the carrier effect of IgG on OT signaling, including OT stability in plasma, OT-R activation, and OT passage to the brain. While the majority of circulating OT is bound to IgG [3], it was not known if IgG may protect OT from degradation by plasma peptidases. IgG protective capacity for OT was tested by a similar approach previously used for ghrelin-binding IgG [37]. For this purpose, a fixed amount of OT (30 fmol) was added to the IgG-deprived pool of plasma samples from BTBR control mice (NaCl) divided into three groups: i) OT with no IgG, ii) OT combined with IgG extracted from plasma samples of BTBR mice receiving adjuvant only (NaCl+Adj), and iii) OT combined with IgG from BTBR mice immunized with *LS* ENO (ENO+Adj). Samples were incubated for 2h at 37°C. OT concentration was measured before (T0) and after incubation, showing its reduction to about 30% in samples without any IgG, and to 50% and 70%, when OT was combined with IgG from the Adj and *LS* ENO-immunized groups, respectively (Fig. 5o). Thus, IgG from the *LS* ENO-immunized mice had superior OT protective properties, enhancing OT stability, possibly underlying increased OT plasma concentration in this study group (Fig. 4h).

IgG from *LS* ENO-immunized mice enhances oxytocin receptor activation

As an OT carrier protein, IgG should not prevent OT-R binding, but may modulate its activation [38]. We thus analyzed the effects of IgG on OT-R activation *in vitro* by β-arrestin recruitment in OT-R-expressing HTLA cells. OT/IgG IC were formed by 0.5 mg/ml of total IgG extracted from plasma of BTBR mice from Exp #3 and 100 nM of synthetic OT, *i.e.,* at the EC_{50} determined for this assay. Application of the OT peptide alone induced OT-R activation with the expected potency (Fig. 5p). Remarkably, the OT IC with IgG from *LS* ENO-immunized mice induced the strongest OT-R activation, which was higher than the IC from other groups and also compared to free OT (Fig. 5p). Higher OT-R activation was also induced by OT IC with IgG from OT-immunized mice as compared to both control groups. Still, it was not different from OT alone. Conversely, IgG from the control groups attenuated OT-R activation (Fig. 5p). As a specificity control of IC effects, the IgG extracts applied alone did not show any signal (data not shown). Thus, these results demonstrate a modulatory effect of OT-binding IgG on OT-R activation, which was most pronounced in IgG from *LS* ENO-immunized mice showing enhanced activation.

IgG transports oxytocin to the brain

Increased OT levels in the brain of *LS* ENO-immunized mice, which was not accompanied by increased OT mRNA expression, but by increased OT-binding IgG levels in the hypothalamus, suggests a carrier role of IgG for OT transportation into the brain. To test this possibility, in a new experiment (Exp #4, Ext. Data Fig. S8d), biotinylated OT (OT-b) was administered via IP injections in three groups of C57Bl6 mice including: i) 10 μg/mL of OT-b alone, ii) OT-b together with IgG purified from plasma of BTBR mice receiving adjuvant (OT-b/IgG NaCl+Adj), or iii) OT-b together with IgG from *LS* ENO-immunized BTBR mice (OT-b/IgG ENO+Adj). In both IgG groups, before injections, 5 μg/mL of IgG was incubated with 10 μg/mL of OT-b overnight to form IC. An additional control group of mice received the same volume, 200 μl of saline as a vehicle. Thirty min after injections, OT-b concentrations were measured in plasma and brain tissue homogenates. We found that mice receiving OT IC with IgG issued from *LS* ENO-immunized BTBR mice had higher OT-b concentrations in plasma (Fig. 5q). OT-b was detected in the brain of mice from all three study groups, with higher levels in the hypothalamus than in the amygdala, while it was not detected in the PFC. In both regions, elevated OT-b concentrations were present in mice receiving the labeled peptide together with IgG from the *LS* ENO-immunized group (Fig. 5r,s). No OT-b signal was detected in any plasma or brain tissues of the control group receiving saline (data not shown). The brain/plasma ratios of OT-b were increased in mice receiving OT-b together with IgG from *LS* ENO-immunized BTBR mice. Such ratios were also higher in the hypothalamus than in the amygdala (Fig. 5t). Thus, these results

revealed the capacity of OT-binding IgG to transport OT into the brain, targeting mainly the hypothalamus and depending on the IgG's OT binding properties; with higher-affinity IgG displaying increased carrier capacity.

Discussion

This study identifies for the first time *LS* ENO as an OT-like systemic bacterial signal, present in human plasma as well as in both the blood and the brain of mice, at levels related to their ASD status. Indeed, the relevance of *LS* ENO to the pathophysiology of ASD was demonstrated by 1) its reduced plasma levels found in infants with ASD starting from the disorder's onset, 2) by its low levels in both blood and brain of BTBR mice, and 3) improved ASD-like behavior when both *LS* ENO and OT concentrations were increased. We propose that, the underlying mechanisms depends on molecular mimicry in *LS* ENO, enabling its interaction with the host OT signaling in two ways: first, as an OT-like antigen-mimetic, inducing OT-binding IgG, which plays the role of an OT carrier protein; and second, as an OT-like ligand weakly activating OT-R (Ext. Data Fig. S11). In the first mechanism, IgG amplifies the endogenous OT signaling by increasing OT stability in the blood, by increasing OT transport from blood to the brain, and by increasing OT-R activation. *LS* ENO-induced IgG boosts OT concentrations in the hypothalamus and amygdala, *i.e.,* in the target brain regions for therapeutic intervention in ASD. The relative contribution of the two mechanisms to the ASD improvement is presently unknown, as our study focused on the OT-like antigenic properties of *LS* ENO.

ENO, also known as phosphopyruvate hydratase, is an enzyme involved in the glycolysis pathway, in its ninth step. The possible connection between this key metabolic pathway generating energy for bacterial growth and the host OT signaling is intriguing. It is tempting to speculate that bacterial growth, stimulated by glucose-rich nutrients, may influence host behavior via stimulation of neurohormonal systems promoting positive feelings and attachment toward such nutrient sources [39]. *LS* ENO is distinct from the neuronal ENO, whose upregulation has been associated with impaired social behavior in ASD mouse models [40]. Maternal antibodies against neuronal ENO have also been associated with ASD in humans [41] and were detected in BTBR mice [32]. Importantly, the detection of *LS* ENO in the brain does not involve neuronal ENO because *LS* ENO was not detected in the brain of germ-free mice. Nevertheless, it cannot be excluded that antibodies binding neuronal ENO may interfere with *LS* ENO via some shared epitopes.

The structural basis of *LS* ENO OT-like properties, both as an antigen and a ligand, appears to depend on the *LS* ENO (24-34) motif displaying three amino acids identical to OT: Tyr^2, Gln^4, and Gly^9. Indeed, in the OT nonapeptide, a disulfide bridge between two cysteines (Cys^1-Cys^6) forms a ring exposing Tyr^2 and Gln^4, which establish hydrogen bonds stabilizing OT in the OT-R binding pocket necessary for receptor activation, while Gly^9 is located close to the receptor surface [42]. In the *LS* ENO (24-34) motif, Tyr and Gln residues are exposed at the tip of a β-sheet formed by the electrostatic forces of the Arg and Glu residues, therefore mimicking the Tyr^2 and Gln^4 duplet in the OT ring. Indeed, AlphaFold modeling [43] of *LS* ENO (24-34) binding to OT-R, shows that this peptide fragment binds the same OT binding pocket, but involves several different interactions (Ext. Data Fig. S12). Notably, the OT-like homology of *LS* ENO was specific to *LS*, suggesting a particular role of this species in modulation of host OT signaling. Nevertheless, detection of OT-like immunoreactivity in other species of lactic bacteria indicates that their ENO and/or other proteins may possess sufficient conformational homology with OT to enable recognition by OT antibodies. The functional significance of such homology is likely related to the antigen-mimetic properties of these proteins, generating a pool of OT-binding IgG antibodies, which may contribute to the probiotic effects of lactic bacteria by increasing OT levels [44,45].

A unique structural homology of *LS* ENO enabling its OT-like ligand features suggests a functional role of *LS* ENO in host physiology, acting both peripherally and in the brain [46]. Although it was not explored in this study, one of *LS* ENO targets may involve gut epithelium known to express OT-R mediating OT anti-inflammatory effects [47,48]. Of possible relevance, increased abundance of *LS* in gut microbiota was associated with improved gastrointestinal symptoms in children with ASD receiving a probiotic mix [49]. *LS* supplementation also had positive effects on social behavior in BTBR mice and anti-depressive effects in rats under chronic mild stress [50,51]. Notably, the establishment of OT signaling in the postnatal period coincides with colonization of the human gut by *Lactobacilli* and *Bifidobacteria*. Of note, OT treatment in a mouse model of ASD has a long-lasting effect in

improving social behavior and normalizing endogenous OT production [52-55]. It would be of interest to determine if *LS* ENO may induce an OT-like neurodevelopmental effect. In this context, a lower potency of OT-R activation by *LS* ENO might not be viewed as a loss of specificity, but as a part of degenerate coding for the neuronal circuit selection during development [56].

We show that it is possible to boost endogenous OT levels in the brain of adult mice by improving the IgG carrier capacity for OT. This finding reveals a so far unknown mechanism in OT physiology, indicating that OT released in circulation from the brain can be recovered with the help of IgG. Moreover, peripheral OT production, *e.g.* in the gut, may potentially contribute to the plasmatic pool of OT [57,58]. Thus, OT-binding IgG may provide an additional supply of OT to the brain regions receiving scarce innervation by the OT neurons, but having dense OT-R expression, *e.g.,* in the amygdala and PFC [59,60]. Indeed, using OT-b, we show that IgG can deliver OT to both the hypothalamus and amygdala. In BTBR mice, low OT levels in the amygdala but high in the hypothalamus suggest impaired innervation of the amygdala by hypothalamic OT neurons. OT in the amygdala is essential for social recognition and modulates affective states in rodents [61,62,63]. It is, hence, likely that boosting OT levels in the amygdala contributed to the improvement of social and anxiety behavior seen in *LS* ENO-immunized BTBR male mice. Sex-differences in behavioral responses, with greater effects observed in males, were also reported after microbial modulation and supplementation of *Limosilactobacillus reuteri* [64,65]. Increased affinity of IgG for OT may underlie superior OT carrier capacity in *LS* ENO-immunized mice. Notably, the basal IgG affinity for OT was lower in BTBR than in C57Bl6 mice, possibly contributing to deficient OT transportation into the brain of BTBR mice. While the exact mechanism of OT brain entry needs further elucidation, it may involve OT-R, whose expression in the brain vascular endothelial cells was recently demonstrated, and the RAGE pathway [66,67]. In addition to increased OT delivery to the brain, IgG with higher affinity for OT increased OT stability in the blood and enhanced OT activation of OT-R. Taken together, improved IgG carrier properties for OT may suffice to stimulate endogenous OT signaling without need for exogenous OT administration. Thus, provision of such IgG as a therapeutic antibody or its induction by *LS* ENO immunization may be suggested as new therapeutic strategies to be explored in ASD.

Indeed, reduced plasma levels of *LS* ENO found in children with ASD justify such approaches. As some children with ASD were analyzed at different time-points, including BOSA negative stages, *i.e.,* still normally developing, we could compare the *LS* ENO dynamics in relation to the establishment of the ASD diagnosis. *LS* ENO levels had striking differences in the same children between BOSA-negative and -positive status, with a significant drop in the latter. These data indirectly suggest a deficient OT-like stimulation by *LS* ENO associated with the ASD onset. Since the ASD diagnosis is typically established after the second BOSA-positive test, low *LS* ENO levels at the first test may serve as an early biomarker of ASD, which should be further validated, considering the geographical differences observed in our cohorts. Further research should also establish what may cause a decrease in *LS* ENO coinciding with ASD onset.

Acknowledgments

The study was supported by “GEMMA”- Genome, Environment, Microbiome & Metabolome in Autism (project ID 825033) funded by the European Commission in the frame of the Horizon 2020 program (call H2020-SC1-BHC-03-2018). We thank all the members of the GEMMA consortium[#] for their role in funding acquisition. S.O.F. was also supported by the Translational Microbiota Program (PTM-2) of Inserm, France. TargEDys SA, France, is acknowledged for providing *Lactobacillus* and *Bifidobacterium* strains and the Biacore T200 instrument. INSERM US51, CNRS UAR 2026, HeRacLeS, was co-supported by European Union and Normandy Region. “Europe gets involved in Normandy with European Regional Development Fund (ERDF)”. Authors thank Julie Maucotel and Axelle Houssier, University of Rouen Normandie, France for the help with animal experimentation. We are grateful to Elizabeth A. Lawson, Harvard Medical School, Boston, USA and Tibor Harkany, Medical University of Vienna, Austria for feedback on the manuscript.

Author contribution

E.L., B.T., designed and performed animal and in vitro experiments, designed *LS* ENO ELISA, analyzed and interpreted data. M.N. designed and performed proteomic experiments. A.L., P.C., L.W., I.O., A.R. and K.D., performed experiments and analyzed data. B.L. synthetized peptides and performed AlphaFold modeling. J.L., A.A. and E.L.C. participated in study design. D.S., S.K. and G.L. performed clinical studies. A.F. designed and coordinated the GEMMA project. S.O.F. conceptualized the project, supervised experiments, analyzed and interpreted data and wrote the manuscript.

Competing Interests

E.L., B.T. and S.O.F. are inventors in a patent application protecting the use of OT-mimetic bacterial proteins (FR2507542, PCT/EP2026/069928). Other co-authors declare no conflict of interest concerning this study.

Methods

Bacterial cultures

Five bacterial strains formerly classified in the genus *Lactobacillus*, and five strains of *Bifidobacteria* (Table 1) were produced by CSL/Sacco (Zelo Buon Persico, Italy) and were provided by TargEDys SA (Longjumeau, France). *Hafnia* (*H.*) *alvei* HA4597 strain was obtained from EnteroSatys® caps (TargEDys) and *E. coli* TG1 strain from the Rouen University laboratory collection. Four aerotolerant *Lactobacillus* strains were cultivated in both aerobic and anaerobic conditions. For aerobic conditions, bacteria were grown overnight in 20 mL of Man Rogosa Sharpe (MRS, BD Difco, 288120) for *Lactobacilli* and *Bifidobacteria* or Luria-Bertani Miller (LB, for *E. coli* and *H. alvei*) broth at 37°C with shaking at 140 rpm. The resulting culture was then diluted to an optical density at 600 nm (OD600) of 0.01, approximately 2×10^6 CFU/mL, in 200 mL of medium. Incubation was continued for 24 hours under the same conditions. For anaerobic conditions, bacteria were cultured overnight in nitrogen-flushed MRS broth in sealed bottles at 37°C without shaking. The culture was then diluted to an OD600 of 0.01 in 200 mL of nitrogen-flushed MRS and incubated for 24 hours under the same anaerobic conditions. The deoxygenation of the MRS medium was verified using the Anaerotest® (Merck, Germany). All cultures were performed in triplicate. For agar culture, a bacterial suspension with a turbidity greater than 4 McFarland units was streaked onto MRS agar plates (BD Difco, 288130, Saint-Ferréol, France). Cultures were incubated at 37 °C in an incubator (Memmert IN110, Schwabach, Germany) for 48 h under either aerobic or anaerobic conditions, the latter using an anaerobic chamber. The deoxygenation of the anaerobic chamber was verified using the Anaerotest® (Merck, Germany).

Table 1: Bacterial strains used in the study

The strains used in this study are listed below, along with their culture mode (medium used and respiratory conditions).

Bacterial strains	Culture mode
***Lacticaseibacillus camelliae* LMG 24277**	MRS, anaerobe
***Lactobacillus gasseri* LG6410**	MRS, aerobe and anaerobe
***Lactiplantibacillus plantarum* 14D**	MRS, aerobe and anaerobe
***Limosilactobacillus reuteri* 92**	MRS, aerobe and anaerobe
***Ligilactobacillus salivarius* LS7892**	MRS, aerobe and anaerobe
***Bifidobacterium adolescentis* Bac30**	MRS, anaerobe
***Bifidobacterium dentium* LMG 11045**	MRS, anaerobe
***Bifidobacterium pseudolongum* subsp. *globosum* LMG 11569**	MRS, anaerobe
***Bifidobacterium pseudolongum* subsp. *pseudolongum* LMG11595**	MRS, anaerobe
***Bifidobacterium ruminantium* LMG21811**	MRS, anaerobe
***Hafnia alvei* 4597**	LB, aerobe
***Escherichia coli* TG1**	LB, aerobe

Bacterial protein extraction

Both aerobic and anaerobic bacterial cultures were centrifuged at 3,000 × g for 20 min at 4°C. The resulting bacterial pellets were washed three times with cold sterile 0.1 M phosphate-buffered saline (PBS, pH 7.4; Sigma-Aldrich, Saint-Quentin-Fallavier, France) and stored at –20 °C overnight. Cell lysis was performed using R2D2 buffer (7 M urea, 2 M thiourea, 2% CHAPS, 0.05% triphosphobutyl, 20 mM dithiothreitol, 0.5% C7BzO): 1 mL for *Bifidobacterium* and 2 mL for *Lactobacillus*. Bacterial pellets were sonicated for 6 minutes at 23%

amplitude (3 seconds ON / 1 second OFF). Proteins were next extracted by centrifugation at 10,000 × g for 10 minutes at 4°C. Soluble (S) and membrane (M) protein fractions were separated from the supernatant by ultracentrifugation at 80,000 × g for 45 min at 4°C. Membrane proteins were resuspended in 100 µL of R2D2 buffer. A second extraction was performed on the remaining bacterial material using the same procedure. Protein concentrations in each fraction—soluble (S), membrane (M), and residual (R)—were determined using the Bradford assay (Bio-Rad).

SDS-PAGE electrophoresis

8 micrograms of protein from each fraction for silver staining and 50 micrograms for western blot (9 samples per strain and condition) were diluted in Laemmli buffer (Bio-Rad) and heated at 95°C for 5 minutes. The samples were then loaded onto a 4–12.5% acrylamide gel, and proteins were separated by SDS-PAGE at a constant current of 10 mA, using molecular weight standards (Thermo Fisher Scientific).

Western Blot and peptide adsorption

Following electrophoresis, proteins were transferred onto a 0.22 µm nitrocellulose membrane (Bio-Rad) using a 25 V current for 10 minutes. Membranes were blocked for 30 minutes in Tris-buffered saline (TBS, pH 7.4; 20 mM Tris base, 0.5 M NaCl, 0.05% Tween 20) containing 5% (w/v) non-fat dry milk (Sigma, St. Louis, USA). After blocking, membranes were incubated overnight with a 1:1000 dilution of polyclonal rabbit anti-OT IgG antibody (Delphi Genetics, Gosselies, Belgium). The membranes were then washed three times with TBS, incubated for 1 hour at room temperature (RT) with a 1:2500 dilution of goat anti-rabbit IgG secondary antibody in milk solution as above (Invitrogen), followed by 3 washes before chemiluminescence detection by a ChemiDoc XRS+ imaging system (BioRad). The most promising fractions and biological replicates were selected for two-dimensional electrophoresis, with at least two technical replicates per biological replicate (4 samples per strain and condition). After revelation, antibodies were dissociated using stripping buffer (Bio-Rad), and the membrane was incubated as previously after adsorption of rabbit anti-OT IgG with 10^{-6} M OT peptide (Bachem AG, Bubendorf, Switzerland).

2-D gel electrophoresis

100 micrograms of protein from selected samples were diluted in isoelectric focusing (IEF) buffer (8 M urea, 65 mM CHAPS, 10 mM DTT, 2% 3–10 NL ampholytes, and 5 µL of 0.2% bromophenol blue) and loaded overnight onto Ready IPG strips (7 cm, pH 3–10 NL; Bio-Rad). The first-dimension electrophoresis was carried out using the Ettan IPGphor 3 System (GE Healthcare) in four steps, totaling 7,000 Vh: 300 V for 1 hour, a gradient to 1,000 V, a gradient to 5,000 V, and 5,000 V for 1 hour. Following IEF, the strips were equilibrated in two successive solutions containing 1.3 mM DTT and 1.3 mM iodoacetamide, respectively. The second-dimension SDS-PAGE was performed on 12.5% acrylamide gels at 10 mA.

Silver staining

For silver staining, proteins were fixed in the gel for 45 minutes at RT using an ethanol/distilled water/acetic acid 30/60/10% solution. The gel was then rinsed in two successive baths of 10% ethanol, followed by two washes in distilled water. The gel was sensitized with 0.002% sodium thiosulfate, stained with 0.1% silver nitrate for 20 minutes, and developed using a solution containing 1.2 g sodium carbonate, 10 µL of 37% formaldehyde, and 4 µL of 2% sodium thiosulfate in 100 mL of distilled water. The staining reaction was stopped with 1% acetic acid.

Intragel trypsin digestion, MS identification and sequence alignment

Protein spots of interest were excised from silver-stained gels and washed with distilled water. Proteins were intra-gel reduced with 5 mM Tris(2-CarboxyEthyl) phosphine hydrochloride (Sigma) in 100 mM ammonium bicarbonate buffer at 56°C for 1h and then alkylated with 55 mM iodoacetamide at RT for 20 min. They were subsequently rinsed with acetonitrile (ACN). Digestion was performed overnight at 37°C using 0.1 µg/µL trypsin (Thermo Scientific) and peptides were extracted using an ACN/5% formic acid (FA) (v:v) solution and dried before MS analysis.

Peptides were analyzed using a nanoLC1200 system coupled to a Q-TOF 6545 XT AdvanceBio mass spectrometer equipped with a nanospray ion source and HPLC-chip cube interface (Agilent Technologies, Les Ulis, France). Samples were first enriched and desalted on a 40 nL RP-C18 trap column, then separated on a Zorbax C18 analytical column (150 mm × 75 µm, 5 µm, 300 Å) using a 26-minute linear gradient of 3–80% ACN in 0.1% FA at a flow rate of 350 nL/min. Mass spectra were acquired in data-dependent mode with full

MS1 scans (290–2000 m/z) and MS2 scans (59–3200 m/z). Up to five doubly or multiply charged precursors were selected per cycle for fragmentation, with singly charged ions excluded. Collision energy was automatically adjusted based on precursor m/z. Dynamic exclusion was applied after one spectrum for 0.2 minutes, with a minimum intensity threshold of 1000 counts.

Protein identification was performed using PEAKS Studio 10.5 (Bioinformatics Solutions Inc.) against the UniProt database. Search parameters included: trypsin specificity with up to three missed cleavages; fixed modification of carbamidomethylation (C); variable modifications including methionine oxidation and pyroglutamate formation from glutamine or glutamic acid; monoisotopic mass selection; precursor mass tolerance of 10 ppm; fragment mass tolerance of 0.05 Da. Only identifications with a false discovery rate (FDR) ≤ 1%, a -logP score ≥ 20, and at least two unique peptides were considered significant. The sequence of identified proteins was aligned with the OT peptide sequence (H-Cys-Tyr-Ile-Gln-Asn-Cys-Pro-Leu-Gly-NH_2) using EMBOSS Needle pairwise sequence alignment tools with the EBLOSUM62 matrix, a gap penalty of 10, and an extended penalty of 0.5. Mismatches and gaps were identified as (); small positive scores were identified as (.); scores > 1 were identified as (:), and identities were identified as (I). Two criteria were used for protein selection: (i) protein recurrence between samples and (ii) OT peptide alignment score. The peptide sequence used for synthesis corresponded to the OT alignment locus.

Peptide and recombinant protein synthesis

OT-like 11-amino acids fragment of *L. salivarius* ENO (24-34) Ac-pEVYTQDGGFGR-NH_2 and *L. gasseri* (LG) ENO-1 (26-36) Ac-FVTLSNGVVGK-NH_2 and ENO-2 (24-34) Ac-EVYTELGGFGR-NH_2 were synthesized by Fmoc solid phase methodology on a Liberty microwave assisted automated peptide synthesizer (CEM, Saclay, France) using the standard manufacturer's procedures at 0.1 mmol scale. All Fmoc-amino acids (0.5 mmol, 5 eq.) were coupled on a Rink amide resin by *in situ* activation with HBTU (0.5 mmol, 5 eq.) and DIEA (1 mmol, 10 eq.) before Fmoc removal with 20% piperidine in DMF. After completion of the chain assembly, peptides were deprotected and cleaved from the resin by adding 10 mL of an ice-cold mixture of TFA/TIS/H_2O (9.5:0.25:0.25, v/v/v) followed by agitation for 3h at RT. After precipitation in TBME followed by centrifugation (4500 rpm, 15 min), the crude peptides were purified by reversed-phase HPLC (Gilson, Villiers le Bel, France) on a 22 x 250 mm Vydac 218TP1022 C_{18}-column (Avantor, Rosny-sous-Bois, France) using a linear gradient (10-50% or 10-40% over 45 min) of acetonitrile/TFA (99.9:0.1) at a flow rate of 10 mL/min. Peptides were then characterized by MALDI-TOF mass spectrometry on an ultrafleXtreme (Bruker, Strasbourg, France) in the reflector mode using α-cyano-4-hydroxycinnamic acid as a matrix. Analytical RP-HPLC, performed on a 4.6 × 250 mm Vydac 218TP54 C_{18}-column, indicated that the purity of the peptides was greater than 99.9%. Recombinant proteins *Ligilactobacillus salivarius* UCC118 ENO (NCBI#Q1WSY0.1), G6PI, and PGK were synthesized by SinoBiologicals (Beijing, P.R. China). *Pseudomonas aeruginosa* EFTU and EFTU antibodies used for Western blot were kindly provided by Marc G.J. Feuilloley, University of Rouen, France.

Animal experiments

Animal care and experimentation complied with both French and European Community regulations (European Community Council Directive of November 24, 1986 (86:609) and were approved by the Normandy Regional Ethics Committee (#37019). Mice were housed under a 12-h light-dark cycle (dark phase: 7:30 PM - 7:30 AM) at 22 °C in standard holding cages (Tecniplast, Buguggiate, Italy), 4-5 animals per cage with *ad libitum* access to a pelleted standard diet (SAFE, Augy, France) and drinking water. Three immunization experiments were performed, two in C57Bl6 mice and one in BTBR mice, and an experiment for OT passage to the brain was performed in C57Bl6 mice as described below.

Exp#1 and #2 in C57Bl6 mice

C57Bl6J 7-week-old male mice were purchased from Janvier Labs (Le Genest-Saint-Isle, France). After 7 days of acclimation to housing conditions, mice were identified using RFID chips injected subcutaneously (Genestil, Royaucourt, France). Blood samples were taken by tail puncture just before immunization. All mice were randomized into 4 (Exp#1) or 6 (Exp#2) groups of 10 mice based on their body weight. Then, mice were IP injected with a 200µL immunization solution consisting of 100% NaCl 0,9% for NaCl group; NaCl 0.9%-CFA (Complete Freund Adjuvant, Sigma) (50:50) (NaCl+Adj), or 50 µg of peptide, recombinant protein, or LS proteome extract mixed in NaCl 0.9%-CFA (50:50). After injection, mice were returned to their holding cages.

2 weeks after the initial immunization, the mice were similarly IP injected with a boost consisting in the same solution switching CFA by IFA (Incomplete Freund Adjuvant, Sigma). One week after, mice were killed by decapitation, trunk blood was collected and stored on ice before plasma separation by centrifugation (2500 g, 20 min at 4°C). Brains were taken and the hypothalamus, prefrontal cortex, and amygdala dissected. All tissue samples were stored on dry ice before being stored in a -80°C freezer until assay.

Exp #3 in BTBR mice

BTBR mice were purchased from Jackson Laboratories and then inbred in the Animal Facility of the University of Rouen Normandie (Breeding agreement #37126). After 7 days of acclimation to experimental housing conditions, 7-week-old mice were identified using RFID chips injected subcutaneously (Genestil, Royaucourt, France). Blood samples were taken by tail puncture just before immunization. All mice were randomized into 6 groups based on their body weight. As previously, mice were IP injected with a 200 µL immunization solution consisting of 100% NaCl 0,9% for the NaCl group; NaCl 0.9%-CFA (Complete Freund Adjuvant, Sigma) (50:50) (NaCl+Adj), or 50 µg of recombinant protein (ENO) mixed in NaCl 0.9%-CFA (50:50). They received a boost injection 2 weeks after, with IFA instead of CFA as adjuvant. Behavioral tests were performed one week after the boost.

Exp #4 in C57Bl6 mice

Biotinylated OT was pre-incubated for 2 h at 37°C in 1X PBS with total IgG purified from BTBR mouse plasma of the Adj group (Freund's adjuvant) or the ENO+Adj group (enolase immunization), at final concentrations of 10 µg/mL of OT and 5 µg/mL of IgG. C57BL6 male mice aged 8 weeks then received 200 µL of the corresponding mixture by intraperitoneal injection. Control mice received 200 µL of 1X PBS, and another control group received 200 µL of biotinylated OT alone. Thirty min after injection, mice were euthanized by decapitation. Blood was collected, and the whole brain was rapidly removed and dissected on a chilled block to isolate the hypothalamus, cortex, and amygdala. Plasma was obtained by centrifugation at 2500 g for 20 min at 4°C. Brain tissues were immediately homogenized in RIPA lysis buffer for protein extraction. Lysis buffer was added at a ratio of 50 µL per mg of tissue, corresponding to approximately 500 µL for 10 mg of tissue. Samples were homogenized until no visible fragments remained, then sonicated on ice using five 5-sec pulses separated by 30-sec intervals to prevent overheating. The homogenates were incubated for 30 min at 4°C with agitation and then centrifuged at 14,000 g for 15 min at 4°C. The supernatants, corresponding to the soluble protein fraction, were carefully collected and transferred to fresh pre-cooled tubes. Protein concentration was determined using the Bradford assay (BioRad).

A polyclonal anti-OT antibody was diluted to 2 µg/mL in coating buffer (0.5 M Na_2CO_3, 0.5 M $NaHCO_3$), and 100 µL per well was added to Maxisorp (Nunc, Rochester, NY, USA) ELISA plates and incubated overnight at 4°C. Plates were washed with 250 µL of wash buffer (PBS supplemented with 0.05% Tween 20). Samples or standards prepared with biotinylated OT were then added at 100 µL per well and incubated for 3 h at 37°C at 120 rpm. After washing, 100 µL of streptavidin-HRP diluted 1:1000 in 1X PBS was added and incubated for 3h at RT under gentle agitation. Wells were washed again, and 100 µL of TMB substrate was added. After 1h of incubation at RT in the dark, the reaction was stopped with 100 µL of 2 N HCl. Absorbance was measured at 450 nm, and concentrations were calculated from the standard curve after blank subtraction.

Oxytocin assay in mouse tissues and oxytocin-like reactivity in bacterial pellets

Oxytocin was quantified in plasma and brain tissues or from 50 mL of anaerobic bacterial cultures (≈ 5.10^9 CFU) with oxytocin ELISA kit (#ADI-901-153A, Enzo Life Sciences, Farmingdale, NY, USA) following manufacturer instructions. After 24 h of culture, bacteria were centrifuged at 3.000 g for 20 min at 4°C and stored overnight at -20°C. Pellets were suspended in 3 mL of PBS 0.1 M and sonicated as described above. Total proteins were recovered by centrifugation at 10.000 x g for 10 min at 4°C, and concentration was quantified by Bradford assay. Three mL of 0.1% TFA was added to the proteome before centrifugation at 13.000 g for 15 min at 4°C. For the brain proteome, tissue was disrupted using a 25G needle and a 1 mL syringe in R2D2 buffer. An equal volume of 0.1% TFA was added to the proteome before centrifugation at 13.000 g for 15 min at 4°C. This proteome (supernatant) was applied to a C18 Sep-Pak column (Waters, Milford, MA, USA) after equilibration with 1 mL ACN and 12 mL 0.1% TFA. Columns were washed with 12 mL 0.1 % TFA, and proteins were slowly eluted (gravity-fed) with 3 mL ACN/TFA 0,1% (95/5). Samples were dried entirely (SpeedVac) and reconstituted with 250 µL of Assay Buffer from the assay kit. 100 microliters of sample were introduced into a 96-well goat anti-rabbit IgG microtiter plate with 50 µL of alkaline phosphatase-conjugated OT and 50 µL of polyclonal rabbit anti-OT IgG. The plate was incubated overnight at

4°C. After 3 washes, the plate was incubated with 200 µL of p-nitrophenylphosphate solution for 1 h at RT. The reaction was stopped and immediately read at an OD of 405 nm. OT-like concentration was estimated in pg/mL using the OT standard range. Protein extracted from bacterial culture grown *Hafnia alvei 4597* (EnteroSatys®, Targedys, France) and from *E. coli* TG1 (laboratory collection) were also analyzed. Strains were compared as OT-positive material (mg) / total extracted proteins (mg) ratios (Figure 1a) or pg/ml. All samples were run in duplicate.

In vitro oxytocin receptor activation assay

Human oxytocin receptor activation was assayed by the PRESTO-TANGO G-protein-coupled receptors β-arrestin recruitment method. The following protocol was adapted from a previous study [68]. HTLA cells were maintained in DMEM supplemented with 10% FBS, 2 µg/mL puromycin, and 100 µg/mL hygromycin B in a humidified atmosphere at 37°C in 5% CO_2. Cells were stably transfected with 2 µg of the Tango-OT-R construct using Lipofectamine 2000 reagent. On day 1, cells were plated on a white 96-well plate at a density of $2x10^4$ cells per well in 90 µL of supplemented DMEM. 6 h later, 10X compounds including oxytocin (Bachem), full-size 48 kDa recombinant LS ENO (SinoBiologicals), ENO (24-34) fragments from LS ENO and from two ENO isoforms of LG, all synthesized as described above, were added at the rate of 10 µL/well, in triplicate. On day 2, the medium and drugs were slowly removed from the wells (aspiration), and 50 µL of 1/20X Bright-Glo luciferase substrate solution (Promega Corporation, Madison, WI, USA, Cat. No. E2620) was added to each well. After 2 min, luminescence was counted with an Infinite F200Pro plate reader (Tecan). Relative luminescence units (RLU) results were exported into Excel sheets, and GraphPad Prism 9 was used for data analysis. To measure constitutive basal activity, no ligand was added. All ligands were assayed 8 times in triplicate. For the analysis of IgG effects on OT-R activation, immune complexes (ICs) of OT with IgG purified from BTBR mouse plasma were assayed in triplicate by adding 0.05 mg of IgG and $10^{-6.5}$ M of OT per well.

Plasma enolase- and oxytocin-binding IgG assay

Plasma levels of ENO- and OT-binding IgG were measured using enzyme-linked immunosorbent assay (ELISA) according to a published protocol [69]. Briefly, recombinant ENO protein (SinoBiological) or OT peptide (Bachem, Bubendorf, Switzerland) was coated onto 96-well Maxisorp plates (Nunc) using 100 µl and a concentration of 2 µg/ml in 0.5 M $NaCO_3$ and 0.5 M $NaHCO_3$ buffer, pH 9.6 for 48 h at 4°C. The plates were washed (3x) in phosphate-buffered saline (PBS) with 0.05% Tween 200, pH 7.4, and then incubated for 3 h at 37°C with 100 µl of mouse plasma diluted to 1:400 in PBS, pH 7.4. The plates were washed (3x) and incubated with 100 µl of alkaline phosphatase-conjugated antibodies in PBS (1:2000, Sigma, St. Louis, MO, USA). Following washing (3x), 200 µl of p-nitrophenyl phosphate solution (Sigma, St. Louis, MO, USA) was added as a substrate. After 30 min of incubation at RT, the reaction was stopped by adding 3N NaOH. The optical density (OD) was determined at 405 nm using a microplate reader Infinite F200PRO (Tecan). Blank OD values resulting from the reading of plates without the addition of plasma samples were subtracted from the sample OD values. Each determination was done in duplicate. The variation between duplicate values was lower than 5%.

Oxytocin-binding IgG assay in the brain

Brain tissue homogenates were prepared as described above in Exp #3. Brain levels of OT-binding IgG were measured according to the same ELISA protocol used for the detection of IgG in plasma shown above. In addition to the assay in tissue samples diluted in PBS, they were also diluted in 3M NaCl, 1.5M glycine pH 8.9 for the analysis of free and total OT-binding IgG, respectively. The percentage of OT-binding IgG present in immune complexes (ICs) was calculated as: 100 – (OD_free / OD_total × 100).

Affinity kinetics of oxytocin-binding IgG

Total IgG was extracted from mouse plasma using MelonGel® Purification Kit (Life Technologies, Carlsbad, CA, USA). IgG concentrations were measured using NanoDrop 2000C (ThermoFisher Scientific, Waltham, MA, USA). Affinity kinetics of IgG for OT were analyzed by biospecific interaction assay (BIA) based on the SPR phenomenon on a BIAcore T200 instrument (Cytiva), according to a previously published protocol [70]. OT was diluted to 0.1 mg/mL in 10 mM sodium acetate buffer, pH 4.5 (Cytiva), and covalently coupled to the CM5 sensor chip (Cytiva). A multi-cycle affinity kinetic analysis method was run with five serial dilutions of purified IgG: 336, 168, 84, 42, 21 nM in HBS-EP+ buffer (0.01 M HEPES pH 7.4, 0.15 M NaCl, 3.0 µM EDTA and 0.05% surfactant P20, Cytiva), each cycle included 120 s of analyte injection and 600 s of dissociation with a 30 µL/min flow speed at 4°C. Between sample injections, the binding surface was regenerated with 10 mM

glycine-HCl buffer pH 2.5, resulting in a return of the baseline level of the sensorgram. Affinity kinetic data were analyzed using the T200 Evaluation 4.1.1 program (Cytiva) and fitted with Langmuir's 1:1 model after blank values subtraction.

Plasma and brain LS ENO assay

For the detection of the LS ENO protein, we developed an enzyme-linked immunosorbent assay (ELISA); for details, see the supplementary figure. For this assay, the recombinant LS ENO protein, as well as anti-ENO rabbit polyclonal and anti-ENO mouse monoclonal antibodies (Abs), were custom-generated by SinoBiological (Beijing, P.R. China). Before the assay, we determined the optimal dilutions of the Abs. We selected a clone that provided a linear detection range for the ENO protein (r=0.98) with an approximately 1 picomolar detection threshold. The specificity of the polyclonal and monoclonal anti-ENO antibodies was confirmed by Western blot. No cross-reactivity of anti-ENO antibodies with OT was detected. Strong LS-ENO-like immunoreactivity was detected in the homogenate of LS, but a weaker signal was also detected in *Limosilactobacillus reuteri* (LR) and *Lacticaseibacillus camelliae* (LC). Other Lactobacillus species, as well as H. alvei and E. coli, had low signal, while no signal was detected in Bifidobacteria (Extended Data, Figure 5). For the LS-ENO detection in plasma and brain homogenates, the polyclonal anti-ENO Abs (2 µg/mL) were coated onto the 96-well Maxisorp plates (Nunc) overnight at 4°C. Plasma samples from both mice and humans were diluted 1/10 in PBS, or 10 µg of total protein extract from mouse brain tissue homogenates was used. Samples were incubated for 2 h at RT, then anti-ENO monoclonal Abs (1:1000) were added for 90 min at RT. Alkaline phosphatase-conjugated anti-mouse Abs (1:2000) (Jackson ImmunoResearch, West Grove, PA, USA) were applied for 90 min at RT. Nitrophenyl phosphate disodium salt hexahydrate (PNPP, Sigma) was used for the chromogenic enzymatic reaction read at the optical density (OD) of 405 nm using a F200Pro spectrophotometer (Tecan).

IgG effect on oxytocin stability in plasma

Plasma from 8 control mice was pooled to obtain a sufficient reaction volume. IgG was purified from this pool using the MelonGel kit (Sigma). The effluent, which did not contain IgG, was collected, thereby representing an IgG-depleted plasma fraction controlled by the absence of IgG detection. The IgG-depleted plasma was then supplemented with 30 fmol of OT in PBS, and the pool was divided into equal-volume reaction samples, including one to control for the initial OT concentration. To assess IgG impact on OT stability, these samples were then supplemented with 1 nmol of purified IgG from individual BTBR mice from different experimental groups. A control condition consisted of OT-containing samples incubated without IgG supplementation. The matrices were then incubated for 2 h at 37 °C. After incubation, OT was measured using an OT ELISA kit (Enzo Life Sciences), according to the manufacturer's instructions. Results are shown as the percentage of OT remaining after 2 h of incubation relative to the initial concentration (T0).

Brain RT-PCR

To assess the gene expression profile in the brain regions and the duodenal mucosa, RNA was extracted. For the brain tissues, a syringe with a 25G needle and lysis buffer supplemented with beta-mercaptoethanol was used to lyse the tissues. For the intestinal mucosa, tissues were disrupted using ceramic beads in a Bioprep-24 Homogenizer (Gentech Biosciences, La Estrella, Colombia). Briefly, 7 beads were added with approximately 30 mg of intestinal mucosa, and then homogenized using the following parameters: 6 m/s, 1 min, repeated twice with a 10-second break. Tissue RNA was next extracted using a NucleoSpin RNA mini kit (Macherey-Nagel, Düren, Germany). Complementary DNA (cDNA) was synthesized using SensiFAST™ cDNA Synthesis Kit with 1 µg of RNA material per sample. Quantitative PCR was performed with QuantStudio 12K Flex (Applied Biosystems, Waltham, MA, USA) in a 384-well plate using SYBR™ Master Mix Fast (Fisher Scientific, Illkirch, France). 384-well plates were filled using the Bravo automated liquid handling platform (Agilent, Santa Clara, CA, USA), with 3.8 µL of master mix and 1.2 µL of diluted cDNA (1/10e). Primers listed in Table 2 were used at 300 nM. The results were analyzed using the delta-delta Ct method, and data are shown as fold levels relative to the expression in the control group of mice.

Table 2. Primer sequences used for RT-qPCR

Symbol	Name	Primer sequence
Actβ	Actin, beta	F: AGGTCATCACTATTGGCAACGA R: CACAGGATTCCATACCCAAGAAG
Gapdh	Glyceraldehyde-3-phosphate dehydrogenase	F: CATGGCCTTCCGTGTTCCTA R: CCTGCTTCACCACCTTCTTGA
Ppia	Peptidylprolyl isomerase A	F: CCACTGTCGCTTTTCGCCGC R: TGCAAACAGCTCGAAGGAGACGC
Bdnf	Brain development neurotrophic factor	F: GCGCCCATGAAAGAAGTAAA R: TCGTCAGACCTCTCGAACCT
Il10	Interleukin 10	F: ATAAGCTCCAAGACCAAGGTGTCT R: ACACACTGCAGGTGTTTTAGCTTTT
Il1β	Interleukin 1 beta	F: GAAGAAGAGCCCATCCTCTGT R: TGTTCATCTCGGAGCCTGTA
Il6	Interleukin 6	F: ACTCCCAACAGACCTGTCTATACCA R: TGCCATTGCACAACTCTTTTCT
Tnfα	Tumor Necrosis Factor alpha	F: CACCGTCAGCCGATTTGC R: TGAGTTGGTCCCCCTTCTCC
Npy	Neuropeptide Y Gene	F: GTGGATCTCTTCTCTCACAG R: CTTGTTACCTAGCATCGTG
Oxt	Oxytocin	F: GACCCTGAGTCTGCCTTCTC R :AAGGTATTCCCAGAAAGTGGGC
Oxtr	Oxytocin receptor	F: TCCACATCTGCACGAAGAAGAA R: CTTCATCATTGTTCTGGCCTTCAT
Pomc	Pro-opiomelanocortin	F: CTCCTGCTTCAGACCTCCATAGA R: GGATGCAAGCCAGCAGGTT

Behavioral tests

Mice were placed in the experimental room 30 min before the start of each behavioral test. After each test, the mouse was returned to its housing cage, any feces were removed, and the arenas were thoroughly wiped. All runs were recorded using Anymaze (version 6.34) with custom setups according to each test. The video tracking was captured from a top-down view of the apparatus.

Three-chambers test

Developed to test social interaction in mice, this test has been largely used in ASD models [71]. The automated three-chamber social approach task quantifies direct social approach behaviors when a study subject mouse is given the choice of spending time in the " social" chamber with a newly introduced mouse (stranger, age- and sex-matched C57Bl6 mice) confined to a restricted enclosure, or of spending time in the 'non-social' chamber where a similar enclosure was placed, but with no animal inside (novel object). The test consisted of three sessions without intertrial intervals. Phase I: The subject mouse was contained in the center chamber for 5 min. Phase II: The subject mouse was allowed to explore the three chambers for 10 min. Phase III: The subject mouse was allowed to explore the three chambers for 10 min, with the stranger mouse in one side chamber and the novel object in the other side chamber. The time spent in each chamber and the time spent exploring the stranger mouse or the novel object in the chamber were automatically recorded using Anymaze and used to assess the sociability of the subject mouse. An exploratory area was defined 2 cm around each restricted enclosure.

Open-field test

Animals were placed individually in the center of a circular, gray plastic open-field container (40 cm diameter) and their spontaneous motor activity was recorded. For each 20-min run (one per mouse), the computer program automatically recorded the following parameters: distance traveled in the center (an area of 20 cm

diameter), periphery, and total, as well as the duration of time spent in the center/inner zone and in the periphery/outer zone.

Elevated plus-maze test

The elevated-plus-maze (EPM) is based on two conflicting innate tendencies: exploring a novel environment and avoiding elevated and open spaces, constituting situations of predator risk. The apparatus consists of two open (stressful) and two enclosed (protective) elevated arms that form a cross (+). The time spent exploring enclosed versus open arms indicates the level of anxiety in the animal. When placed in this apparatus, naïve mice tend to explore the open arms less naturally due to their innate fear of heights and open spaces. In this context, anxiolytics generally increase the time spent exploring the open arms, and anxiogenics have the opposite effect, increasing the time spent in the closed arms. For EPM testing, mice were placed in the center of the maze, facing the inside of a closed arm. The tests were 5 min in duration. An overhead camera linked to computer software tracked the mouse's position and calculated the time spent in the open zones of the maze, as well as the distance traveled during the test.

Self-grooming test

Grooming is a fundamental and evolutionarily conserved behavior observed across a wide range of animal species. While its primary role is maintaining hygiene and caring for the body surface, grooming also fulfills several additional functions. These include skin stimulation, thermoregulation, chemical communication, social bonding, emotional calming, and stress relief. The arena consisted of a rat open field divided into four equal 12 cm-square sides. Mice were isolated in this compartment for 20 minutes, with the first 10 min serving as a habituation phase. During the last 10 min, grooming episodes, as well as latencies before the first grooming and total grooming duration, were video-recorded.

Study subjects

Informed consent was obtained from all parents of subjects enrolled in this study in compliance with national legislation and the Code of Ethical Principles for Medical Research Involving Human Subjects of the World Medical Association (Declaration of Helsinki). Three recruitment centers located in Italy, USA, and Ireland were engaged in the Genome, Environment, Microbiome & Metabolome in Autism “GEMMA project” 2021-SC1-BHC-2018 #825033. The study was approved by the respective local ethical committees. Azienda Sanitaria Locale (ASL) Napoli 3 Sud IRB, Italy, approval n. 30 05/03/2019 (observational trial). Mass General Brigham IRB, USA, Protocol #2018P002109 and GalwayCclinical Research Ethics Committee, Ireland, Ref.: C.A.2127. Within the GEMMA cohort, we investigated 52 (28 boys and 24 girls) newly diagnosed children with ASD and compared them to 39 (20 boys and 19 girls) age- and sex-matched healthy children used as a Control group). Fresh peripheral blood samples from ASD subjects and control donors were drawn and collected in sterile EDTA tubes. To minimize stress in children, we adopted a small-sized protocol for blood withdrawal [72].

Statistical analysis

Data were analyzed, and the graphs were plotted using GraphPad Prism 9.0. (GraphPad Software Inc., San Diego, CA). Individual groups were compared with the Student’s t-test, and the changes in the same groups were compared with the paired t-test or Wilcoxon’s test. Multiple groups were compared with ANOVA and Tukey’s post-test or by Kruskal-Wallis with Dunn’s post-test, according to normality analyzed by the Kolmogorov-Smirnov’s test. Correlations were analyzed using Pearson’s or Spearman’s tests, according to normality. Data are shown as means ± standard error of means (SEM), and for all tests, $p < 0.05$ was considered statistically significant.

References

1 Boulton, K. A. & Guastella, A. J. Oxytocin and autism - A precision medicine framework to unpack mechanisms and evidence. *Neurosci Biobehav Rev* **187**, 106746, doi:10.1016/j.neubiorev.2026.106746 (2026).

2 Fang, G., Pan, W., Li, G., Ma, L. & Wei, J. The Effect of Intranasal Oxytocin on Social Interaction in Adults and Children With Autism Spectrum Disorders: A Systematic Review and Meta-analysis of Randomized Controlled Trials. *Alpha Psychiatry* **27**, 45322, doi:10.31083/ap45322 (2026).

3 Værøy, H. *et al.* Immunoglobulin G is a natural oxytocin carrier which modulates oxytocin receptor signaling: relevance to aggressive behavior in humans. *Discover Mental Health* **3**, 21, doi:10.1007/s44192-023-00048-z (2023).

4 Carter, C. S. *et al.* Is Oxytocin "Nature's Medicine"? *Pharmacol Rev* **72**, 829-861, doi:10.1124/pr.120.019398 (2020).

5 Lawson, E. A. Understanding oxytocin in human physiology and pathophysiology: A path towards therapeutics. *Comprehensive Psychoneuroendocrinology* **19**, 100242, doi:https://doi.org/10.1016/j.cpnec.2024.100242 (2024).

6 Dromard, Y. *et al.* Disengagement of somatostatin neurons from lateral septum circuitry by oxytocin and vasopressin restores social-fear extinction and suppresses aggression outbursts in Prader-Willi syndrome model. *Biol Psychiatry* **95**, 785-799, doi:10.1016/j.biopsych.2023.10.016 (2024).

7 de Jong, T. R. & Neumann, I. D. Oxytocin and aggression. *Curr Top Behav Neurosci* **35**, 175-192, doi:10.1007/7854_2017_13 (2018).

8 Muscatelli, F., Desarménien, M. G., Matarazzo, V. & Grinevich, V. 1-30 (Springer Berlin Heidelberg, 2017).

9 Harkany, T., Hevesi, Z. & Hökfelt, T. Neuropeptide receptors as entry points for developmental vulnerability to drug abuse. *Current Opinion in Neurobiology* **95**, 103125, doi:https://doi.org/10.1016/j.conb.2025.103125 (2025).

10 Kingsbury, M. A. & Bilbo, S. D. The inflammatory event of birth: How oxytocin signaling may guide the development of the brain and gastrointestinal system. *Front Neuroendocrinol* **55**, 100794, doi:10.1016/j.yfrne.2019.100794 (2019).

11 Guastella, A. J. & Hickie, I. B. Oxytocin Treatment, Circuitry, and Autism: A Critical Review of the Literature Placing Oxytocin Into the Autism Context. *Biol Psychiatry* **79**, 234-242, doi:10.1016/j.biopsych.2015.06.028 (2016).

12 Andari, E. *et al.* Promoting social behavior with oxytocin in high-functioning autism spectrum disorders. *Proc Natl Acad Sci U S A* **107**, 4389-4394, doi:10.1073/pnas.0910249107 (2010).

13 Lal, N. *et al.* An overview of oxytocin integrative mechanisms in autism spectrum disorder. *Discov Ment Health* **5**, 185, doi:10.1007/s44192-025-00331-1 (2025).

14 Guastella, A. J. *et al.* The effect of oxytocin nasal spray on social interaction in young children with autism: a randomized clinical trial. *Mol Psychiatry* **28**, 834-842, doi:10.1038/s41380-022-01845-8 (2023).

15 Daniels, N. *et al.* Effects of multiple-dose intranasal oxytocin administration on social responsiveness in children with autism: a randomized, placebo-controlled trial. *Mol Autism* **14**, 16, doi:10.1186/s13229-023-00546-5 (2023).

16 Romney, C., Hahn-Holbrook, J., Norman, G. J., Moore, A. & Holt-Lunstad, J. Where is the love? A double-blind, randomized study of the effects of intranasal oxytocin on stress regulation and aggression. *Int J Psychophysiol* **136**, 15-21, doi:10.1016/j.ijpsycho.2018.08.010 (2019).

17 Leng, G. & Ludwig, M. Intranasal Oxytocin: Myths and Delusions. *Biological Psychiatry* **79**, 243-250, doi:https://doi.org/10.1016/j.biopsych.2015.05.003 (2016).

18 Boulton, K. A. & Guastella, A. J. Oxytocin and autism – A precision medicine framework to unpack mechanisms and evidence. *Neuroscience & Biobehavioral Reviews* **187**, 106746, doi:https://doi.org/10.1016/j.neubiorev.2026.106746 (2026).

19 Oldstone, M. B. Molecular mimicry, microbial infection, and autoimmune disease: evolution of the concept. *Curr Top Microbiol Immunol* **296**, 1-17 (2005).

20 Rutayisire, E., Huang, K., Liu, Y. & Tao, F. The mode of delivery affects the diversity and colonization pattern of the gut microbiota during the first year of infants' life: a systematic review. *BMC Gastroenterol* **16**, 86, doi:10.1186/s12876-016-0498-0 (2016).
21 Samarra, A. *et al.* Human milk oligosaccharide metabolism and antibiotic resistance in early gut colonizers: insights from bifidobacteria and lactobacilli in the maternal-infant microbiome. *Gut Microbes* **17**, 2501192, doi:10.1080/19490976.2025.2501192 (2025).
22 Diaz Heijtz, R. *et al.* Normal gut microbiota modulates brain development and behavior. *Proc Natl Acad Sci U S A* **108**, 3047-3052, doi:10.1073/pnas.1010529108 (2011).
23 O'Riordan, K. J., Aburto, M. R., Nagpal, J., Clarke, G. & Cryan, J. F. Microbiome: A Key Regulator of Body-Brain Interactions. *Adv Exp Med Biol* **1477**, 139-203, doi:10.1007/978-3-031-89525-8_6 (2025).
24 Sharon, G. *et al.* Human Gut Microbiota from Autism Spectrum Disorder Promote Behavioral Symptoms in Mice. *Cell* **177**, 1600-1618.e1617, doi:10.1016/j.cell.2019.05.004 (2019).
25 Mazzone, L. *et al.* Precision microbial intervention improves social behavior but not autism severity: A pilot double-blind randomized placebo-controlled trial. *Cell Host & Microbe* **32**, 106-116.e106, doi:10.1016/j.chom.2023.11.021 (2024).
26 Sgritta, M. *et al.* Mechanisms Underlying Microbial-Mediated Changes in Social Behavior in Mouse Models of Autism Spectrum Disorder. *Neuron* **101**, 246-259.e246, doi:10.1016/j.neuron.2018.11.018 (2019).
27 Yang, Y. *et al.* Understanding Ligilactobacillus salivarius from Probiotic Properties to Omics Technology: A Review. *Foods* **13**, doi:10.3390/foods13060895 (2024).
28 Nicol, M. *et al.* Lactobacillus salivarius and Lactobacillus gasseri supplementation reduces stress-induced sugar craving in mice. *European Eating Disorders Review*, doi:https://doi.org/10.1002/erv.3004 (2023).
29 Troisi, J. *et al.* Genome, Environment, Microbiome and Metabolome in Autism (GEMMA) Study Design: Biomarkers Identification for Precision Treatment and Primary Prevention of Autism Spectrum Disorders by an Integrated Multi-Omics Systems Biology Approach. *Brain Sci* **10**, doi:10.3390/brainsci10100743 (2020).
30 Meyza, K. Z. & Blanchard, D. C. The BTBR mouse model of idiopathic autism - Current view on mechanisms. *Neurosci Biobehav Rev* **76**, 99-110, doi:10.1016/j.neubiorev.2016.12.037 (2017).
31 Schwartzer, J. J. *et al.* Maternal immune activation and strain specific interactions in the development of autism-like behaviors in mice. *Transl Psychiatry* **3**, e240, doi:10.1038/tp.2013.16 (2013).
32 Uddin, M. N. *et al.* Immunity and autoantibodies of a mouse strain with autistic-like behavior. *Brain, Behavior, & Immunity - Health* **4**, 100069, doi:https://doi.org/10.1016/j.bbih.2020.100069 (2020).
33 de Leão, E. *et al.* Lateral septum microglial changes and behavioral abnormalities of mice exposed to valproic acid during the prenatal period. *J Chem Neuroanat* **111**, 101875, doi:10.1016/j.jchemneu.2020.101875 (2021).
34 Arakawa, H., Higuchi, Y. & Ozawa, A. Oxytocin neurons in the paraventricular nucleus of the hypothalamus circuit-dependently regulates social behavior, which malfunctions in BTBR mouse model of autism. *Res Sq*, doi:10.21203/rs.3.rs-2621359/v1 (2023).
35 Tapp, D. N., Singstock, M. D., Gottliebson, M. S. & McMurray, M. S. Central but not peripheral oxytocin administration reduces risk-based decision-making in male rats. *Horm Behav* **125**, 104840, doi:10.1016/j.yhbeh.2020.104840 (2020).
36 Bozorgmehr, A. *et al.* Oxytocin moderates risky decision-making during the Iowa Gambling Task: A new insight based on the role of oxytocin receptor gene polymorphisms and interventional cognitive study. *Neurosci Lett* **708**, 134328, doi:10.1016/j.neulet.2019.134328 (2019).
37 Takagi, K. *et al.* Anti-ghrelin immunoglobulins modulate ghrelin stability and its orexigenic effect in obese mice and humans. *Nat Commun* **4**, 2685 (2013).
38 Lahaye, E. & Fetissov, S. O. Functional role of immunoglobulin G as an oxytocin-carrier protein. *Peptides* **177**, 171221, doi:10.1016/j.peptides.2024.171221 (2024).
39 Coria-Avila, G. A. *et al.* Neurobiology of social attachments. *Neurosci Biobehav Rev* **43**, 173-182, doi:10.1016/j.neubiorev.2014.04.004 (2014).

40 Wang, M. *et al.* Axin2 coupled excessive Wnt-glycolysis signaling mediates social defect in autism spectrum disorders. *EMBO Molecular Medicine* **15**, EMMM202217101, doi:10.15252/emmm.202217101 (2023).
41 Ramirez-Celis, A., Edmiston, E., Schauer, J., Vu, T. & Van de Water, J. Peptides of neuron specific enolase as potential ASD biomarkers: From discovery to epitope mapping. *Brain, Behavior, and Immunity* **84**, 200-208, doi:https://doi.org/10.1016/j.bbi.2019.12.002 (2020).
42 Waltenspühl, Y. *et al.* Structural basis for the activation and ligand recognition of the human oxytocin receptor. *Nat Commun* **13**, 4153, doi:10.1038/s41467-022-31325-0 (2022).
43 Mirdita, M. *et al.* ColabFold: making protein folding accessible to all. *Nature methods* **19**, 679-682, doi:10.1038/s41592-022-01488-1 (2022).
44 Varian, B. J. *et al.* Microbial lysate upregulates host oxytocin. *Brain, Behavior, and Immunity* **61**, 36-49, doi:https://doi.org/10.1016/j.bbi.2016.11.002 (2017).
45 Benlakehal, R. *et al.* Probiotic L. reuteri treatment in stressed rats improves maternal care and corrects corticosterone-BDNF-oxytocin balance offering insights for maternal postpartum distress treatment. *Scientific reports* **15**, 23544, doi:10.1038/s41598-025-05848-7 (2025).
46 Greenwood, M. A. & Hammock, E. A. Oxytocin receptor binding sites in the periphery of the neonatal mouse. *PLoS One* **12**, e0172904, doi:10.1371/journal.pone.0172904 (2017).
47 Welch, M. G. *et al.* Expression and developmental regulation of oxytocin (OT) and oxytocin receptors (OTR) in the enteric nervous system (ENS) and intestinal epithelium. *Journal of Comparative Neurology* **512**, 256-270, doi:10.1002/cne.21872 (2009).
48 Klein, B. Y. *et al.* Oxytocin opposes effects of bacterial endotoxin on ER-stress signaling in Caco2BB gut cells. *Biochim Biophys Acta* **1860**, 402-411, doi:10.1016/j.bbagen.2015.10.025 (2016).
49 Guidetti, C. *et al.* Randomized Double-Blind Crossover Study for Evaluating a Probiotic Mixture on Gastrointestinal and Behavioral Symptoms of Autistic Children. *J Clin Med* **11**, doi:10.3390/jcm11185263 (2022).
50 Pochakom, A. *et al.* Selective Probiotic Treatment Positively Modulates the Microbiota–Gut–Brain Axis in the BTBR Mouse Model of Autism. *Brain Sciences* **12**, 781 (2022).
51 Martín-Hernández, D. *et al.* Behavioral, antioxidant, and kynurenine pathway modulation of a specific strain of Ligilactobacillus salivarius in a preclinical model of depression. *Eur J Nutr* **65**, doi:10.1007/s00394-026-03941-9 (2026).
52 Bealer, S. L., Lipschitz, D. L., Ramoz, G. & Crowley, W. R. Oxytocin receptor binding in the hypothalamus during gestation in rats. *American Journal of Physiology-Regulatory, Integrative and Comparative Physiology* **291**, R53-R58, doi:10.1152/ajpregu.00766.2005 (2006).
53 Peñagarikano, O. *et al.* Exogenous and evoked oxytocin restores social behavior in the *Cntnap2* mouse model of autism. *Science Translational Medicine* **7**, 271ra278-271ra278, doi:10.1126/scitranslmed.3010257 (2015).
54 Muscatelli, F., Matarazzo, V. & Chini, B. Neonatal oxytocin gives the tempo of social and feeding behaviors. *Front Mol Neurosci* **15**, 1071719, doi:10.3389/fnmol.2022.1071719 (2022).
55 Zhang, F., Xu, W., Zeng, R., Chen, J. & Huang, J. Limosilactobacillus reuteri normalizes gut microbiota dysfunction and social deficits of rat offspring associated with prenatal exposure to stress. *Gut Microbes* **18**, 2649440, doi:10.1080/19490976.2026.2649440 (2026).
56 Edelman, G. M. Neural Darwinism: selection and reentrant signaling in higher brain function. *Neuron* **10**, 115-125, doi:10.1016/0896-6273(93)90304-a (1993).
57 Danhof, H. A., Lee, J., Thapa, A., Britton, R. A. & Di Rienzi, S. C. Microbial stimulation of oxytocin release from the intestinal epithelium via secretin signaling. *Gut Microbes* **15**, 2256043, doi:10.1080/19490976.2023.2256043 (2023).
58 Gether, I. M. *et al.* Oxytocin mRNA is expressed throughout the small intestine in individuals with and without type 2 diabetes, and circulating neurophysin I declines after Roux-en-Y gastric bypass surgery. *Diabetes, Obesity and Metabolism* **27**, 5373-5377, doi:https://doi.org/10.1111/dom.16571 (2025).
59 Liao, P.-Y., Chiu, Y.-M., Yu, J.-H. & Chen, S.-K. Mapping Central Projection of Oxytocin Neurons in Unmated Mice Using Cre and Alkaline Phosphatase Reporter. *Frontiers in Neuroanatomy* **Volume 14 - 2020**, doi:10.3389/fnana.2020.559402 (2020).

60 Schimmer, S. *et al.* Oxytocin facilitates social behavior of female rats via selective modulation of interneurons in the medial prefrontal cortex. *Nat Commun* **17**, doi:10.1038/s41467-026-68347-x (2026).
61 Higuchi, Y., Tachigori, S.-i. & Arakawa, H. Faded neural projection from the posterior bed nucleus of the stria terminalis to the lateral habenula contributes to social signaling deficit in male BTBR mice as a mouse model of autism. *Psychoneuroendocrinology* **149**, 106004, doi:https://doi.org/10.1016/j.psyneuen.2022.106004 (2023).
62 Ferguson, J. N., Aldag, J. M., Insel, T. R. & Young, L. J. Oxytocin in the Medial Amygdala is Essential for Social Recognition in the Mouse. *The Journal of Neuroscience* **21**, 8278-8285, doi:10.1523/jneurosci.21-20-08278.2001 (2001).
63 Wahis, J. *et al.* Astrocytes mediate the effect of oxytocin in the central amygdala on neuronal activity and affective states in rodents. *Nat Neurosci* **24**, 529-541, doi:10.1038/s41593-021-00800-0 (2021).
64 Siegler Lathrop, T., Martínez Sanchez, I., Chronakis, I. S. & Diaz Heijtz, R. Sex-Specific Long-Term Effects of Perinatal Limosilactobacillus reuteri on Social Cognition, Gene Expression, and Gut Microbiota. *J Neurochem* **169**, e70199, doi:10.1111/jnc.70199 (2025).
65 Smith, C. J. *et al.* Microbial modulation via cross-fostering prevents the effects of pervasive environmental stressors on microglia and social behavior, but not the dopamine system. *Mol Psychiatry* **28**, 2549-2562, doi:10.1038/s41380-023-02108-w (2023).
66 Paolini, C., Piacentini, F., Amato, S., Busnelli, M. & Chini, B. Oxytocin supports the barrier integrity of brain endothelial cells via oxytocin receptors. *J Neuroendocrinol* **38**, e70152, doi:10.1111/jne.70152 (2026).
67 Yamamoto, Y. & Higashida, H. RAGE regulates oxytocin transport into the brain. *Communications Biology* **3**, 70, doi:10.1038/s42003-020-0799-2 (2020).
68 Duraisamy, K. *et al.* MRGPRB2/X2 and the analogous effects of its agonist and antagonist in DSS-induced colitis in mice. *Biomedicine & Pharmacotherapy* **174**, 116471, doi:https://doi.org/10.1016/j.biopha.2024.116471 (2024).
69 Fetissov, S. O. Neuropeptide autoantibodies assay. *Methods Mol Biol* **789**, 295-302 (2011).
70 Legrand, R., Takagi, K. & Fetissov, S. O. Immunoglobulin G preparation from plasma samples and analysis of its affinity kinetic binding to peptide hormones. *Protocol Exchange* **doi:10.1038/protex.2014.004** (2014).
71 Nadler, J. J. *et al.* Automated apparatus for quantitation of social approach behaviors in mice. *Genes, brain, and behavior* **3**, 303-314, doi:10.1111/j.1601-183X.2004.00071.x (2004).
72 Patrone, D. *et al.* Optimization of Peripheral Blood Mononuclear Cell Extraction from Small Volume of Blood Samples: Potential Implications for Children-Related Diseases. *Methods and Protocols* **5**, 20 (2022).

Extended Data

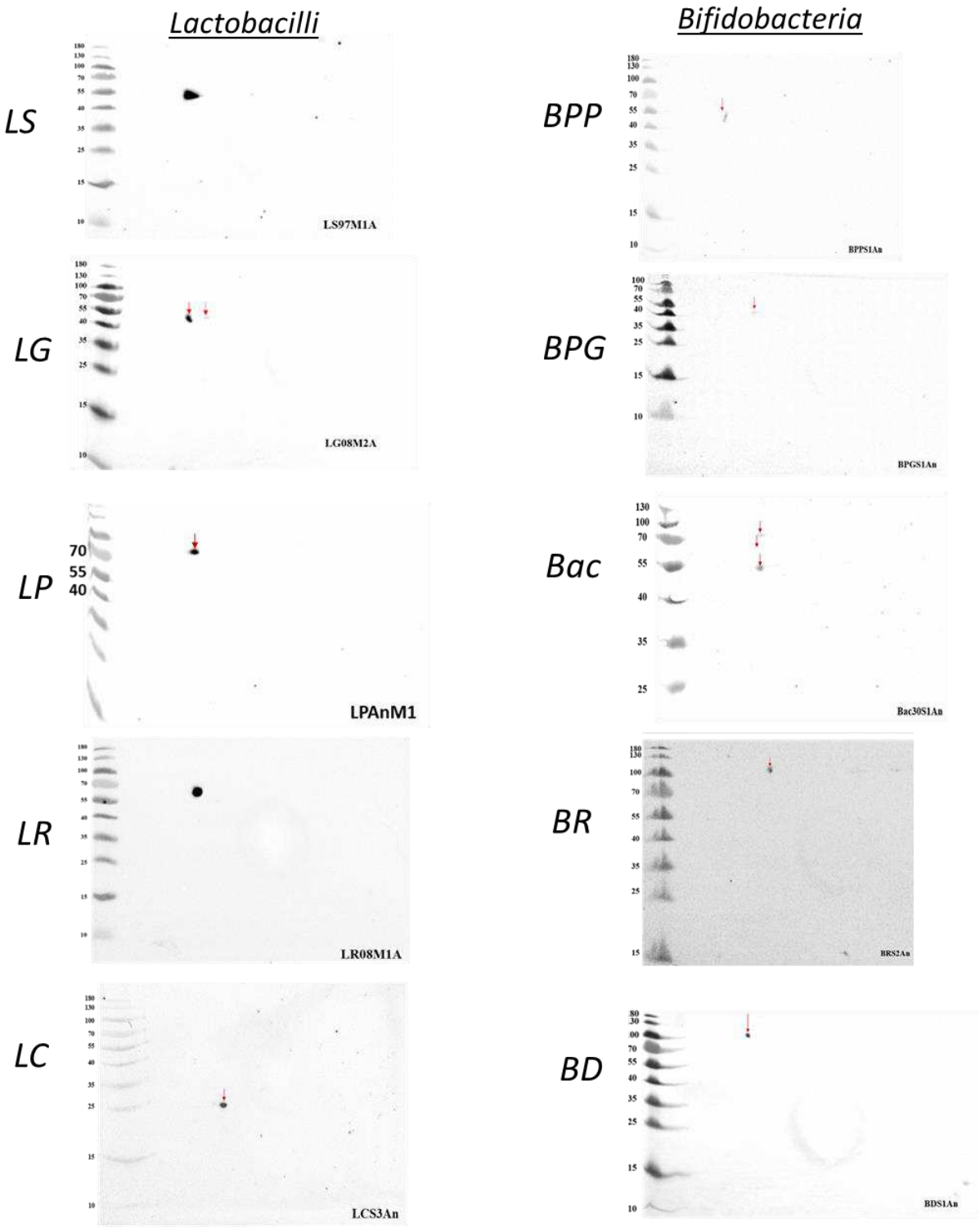


Figure S1. Initial screening for the presence of OT-like cross-reactivity in lactic bacteria species by 2DGE followed by immunodetection with polyclonal OT antibodies. Tested *Lactobacilli* (left column): *Ligilactobacillus salivarius* (*LS*)*, Lactobacillus gasseri* (*LG*), *Lactiplantibacillus plantarum* (*LP*)*, Limosilactobacillus reuteri* (*LR*), and *Lacticaseibacillus camelliae* (*LC*). Tested *Bifidobacterium* (*B*) species (right column): *B. pseudolongum* subsp. *pseudolongum* (*BPP*)*, B. pseudolongum* subsp. *globosum* (*BPG*)*, B. adolescentis* (*Bac*), *B. ruminantium* (*BR*), and *B. dentium* (*BD*). Red arrows point to OT-like immunopositive spots. Each blot has a unique code defining the cellular fraction, growth condition, and sample number used.

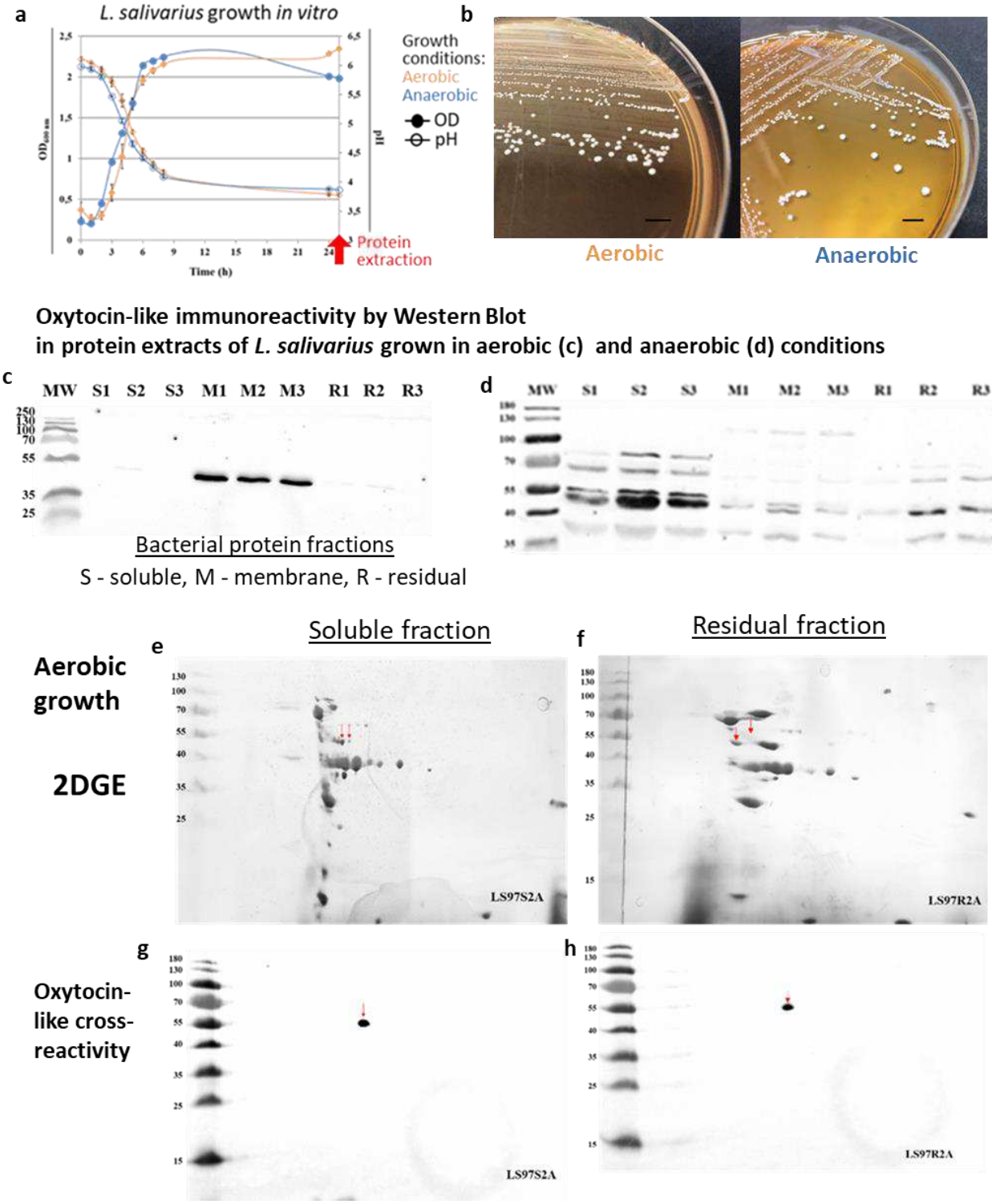


Figure S2. 2DGE, immunodetection, and mass spectrometry identification of oxytocin-like spots in *L. salivarius)* cultivated in aerobic conditions. Growth of *LS* in planktonic (**a**) and agar (**b**) cultures in aerobic and anaerobic conditions. **c,d**. OT Western blot of *LS* three subcellular protein fractions, soluble (S), membrane (M) and residual (R), after bacterial growth in aerobic (**c**) and anaerobic (**d**) conditions, each culture repeated in three independent experiments (1,2,3). 2D gel electrophoresis (2DGE) profile of the soluble (**e**) and residual (**f**) protein fractions of *LS* grown under aerobic conditions, followed by the transfer to a nitrocellulose membrane and immunodetection with polyclonal OT IgG in each fraction, respectively (**g,h**). Red arrows indicate the protein spots detected by OT IgG on the corresponding membranes.

OT-like positive spot 1 from residual fraction

Accession	-10lgP	Coverage (%)	#Peptides	#Unique	PTM	Avg. Mass	Description
ENO_LACS1	676.23	89	28	28	Y	48052	Enolase
MTLD_LACS1	498.68	51	17	17	Y	42778	Mannitol-1-phosphate 5-dehydrogenase
G6PI_LACS1	390.10	28	7	6	Y	49947	Glucose-6-phosphate isomerase
EFTU_LACS1	281.59	17	4	4	N	43274	Elongation factor Tu
PGK_LACS1	157.20	12	4	4	N	42647	Phosphoglycerate kinase

OT-like positive spot 2 from residual fraction

Accession	-10lgP	Coverage (%)	#Peptides	#Unique	PTM	Avg. Mass	Description
ENO_LACS1	480.30	42	13	13	N	48052	Enolase
G6PI_LACS1	460.61	44	16	16	N	49947	Glucose-6-phosphate isomerase
EFTU_LACS1	394.46	38	12	12	N	43274	Elongation factor Tu
MTLD_LACS1	196.20	11	4	4	N	42778	Mannitol-1-phosphate 5-dehydrogenase
CH60_LACS1	101.93	5	2	2	N	57352	60 kDa chaperonin

OT-like positive spot from membrane fraction

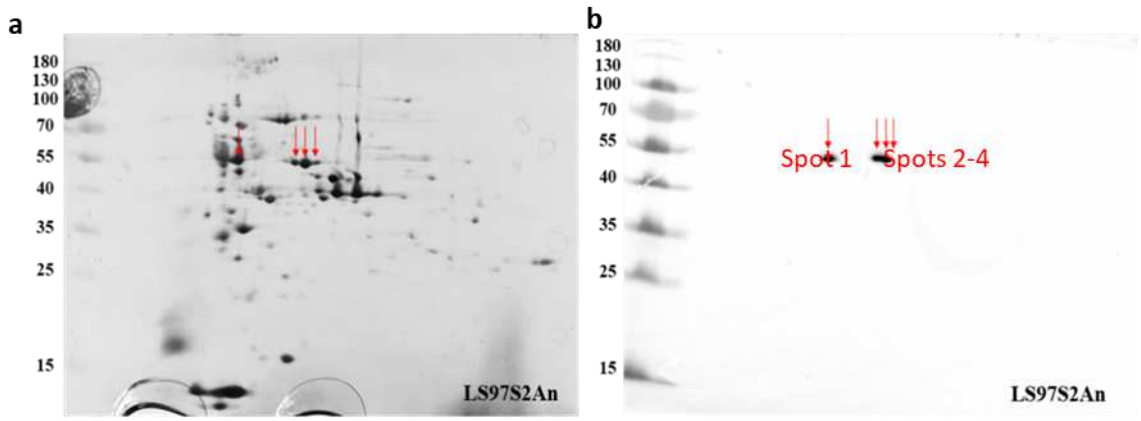
Accession	-10lgP	Coverage (%)	#Peptides	#Unique	PTM	Avg. Mass	Description
ENO_LACS1	246.34	81	49	34	Y	48052	Enolase
MTLD_LACS1	116.65	19	7	7	N	42778	Mannitol-1-phosphate 5-dehydrogenase
PGK_LACS1	31.78	5	2	2	N	42647	Phosphoglycerate kinase

Accession	-10lgP	Coverage (%)	#Peptides	#Unique	PTM	Avg. Mass	Description
ENO_LACS1	269.68	78	41	26	Y	48052	Enolase
DDL_LACS1	204.41	48	18	18	Y	42553	D-alanine--D-alanine ligase
MTLD_LACS1	151.38	43	14	14	N	42778	Mannitol-1-phosphate 5-dehydrogenase
EFTU_LACS1	148.87	22	6	6	N	43274	Elongation factor Tu
G6PI_LACS1	88.35	14	5	5	N	49947	Glucose-6-phosphate isomerase

OT-like positive spot from soluble fraction

Accession	-10lgP	Coverage (%)	#Peptides	#Unique	PTM	Avg. Mass	Description
PGK_LACS1	371.43	85	28	23	Y	42647	Phosphoglycerate kinase
ENO_LACS1	281.27	30	9	9	N	48052	Enolase
PYRC_LACS1	140.22	11	4	4	Y	46735	Dihydroorotase

Figure S3. Mass spectrometry identification of oxytocin-like spots in residual, membrane and soluble fractions of aerobically grown *L. salivarius*. The tables show the proteins identified in OT-like immunopositive spots of different *LS* fractions, including the corresponding identification parameters.



c. OT-like positive Spot 1

Accession	-10lgP	Coverage (%)	#Peptides	#Unique	PTM	Avg. Mass	Description
EFTU_LACGA	254.88	91	58	6	Y	43677	Elongation factor Tu
G6PI_LACGA	180.50	52	23	23	N	49857	Glucose-6-phosphate isomerase
ENO1_LACGA	177.36	49	16	16	Y	46652	Enolase 1
ENO2_LACGA	139.56	35	10	10	N	46911	Enolase 2
DDL_LACGA	60.70	7	3	3	N	40401	D-alanine—D-alanine ligase
RF1_LACGA	58.27	7	2	2	N	41541	Peptide chain release factor 1
EFG_LACGA	46.13	4	2	2	N	76948	Elongation factor G

d. OT-like positive Spots 2-4

Accession	-10lgP	Coverage (%)	#Peptides	#Unique	PTM	Avg. Mass	Description
PGK_LACGA	225.32 226.45 214.18	79 80 80	38 38 41	18 15 18	Y	43043	Phosphoglycerate kinase
CLPX_LACGA	132.18 95.74 -	23 14 -	8 5 -	8 5 -	N	46553	ATP-dependent Clp protease ATP-binding subunit ClpX

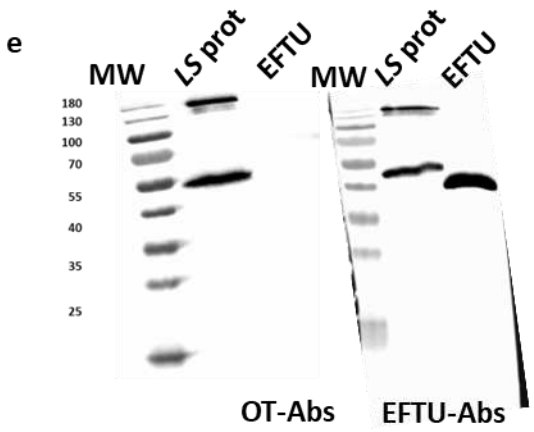


Figure S4. **2DGE, immunodetection, and mass spectrometry identification of oxytocin-like spots in *L. salivarius (LS)* cultivated in anaerobic conditions. a.** 2DGE profile of the soluble cellular protein fraction extracted from *LS*. **b.** Immunodetection of the corresponding 2D gel using a polyclonal anti-OT antibody. Red arrows indicate OT-like protein spots. The two tables report the mass spectrometry identification of proteins corresponding to spot 1 (**c**) and spots 2–4 (**d**). **e.** Western blot of *Pseudomonas aeruginosa* elongation factor Tu (EFTU) was revealed with OT and EFTU antibodies. *LS* total protein extract (*LS* prot) was used as a positive control for OT-like reactivity.

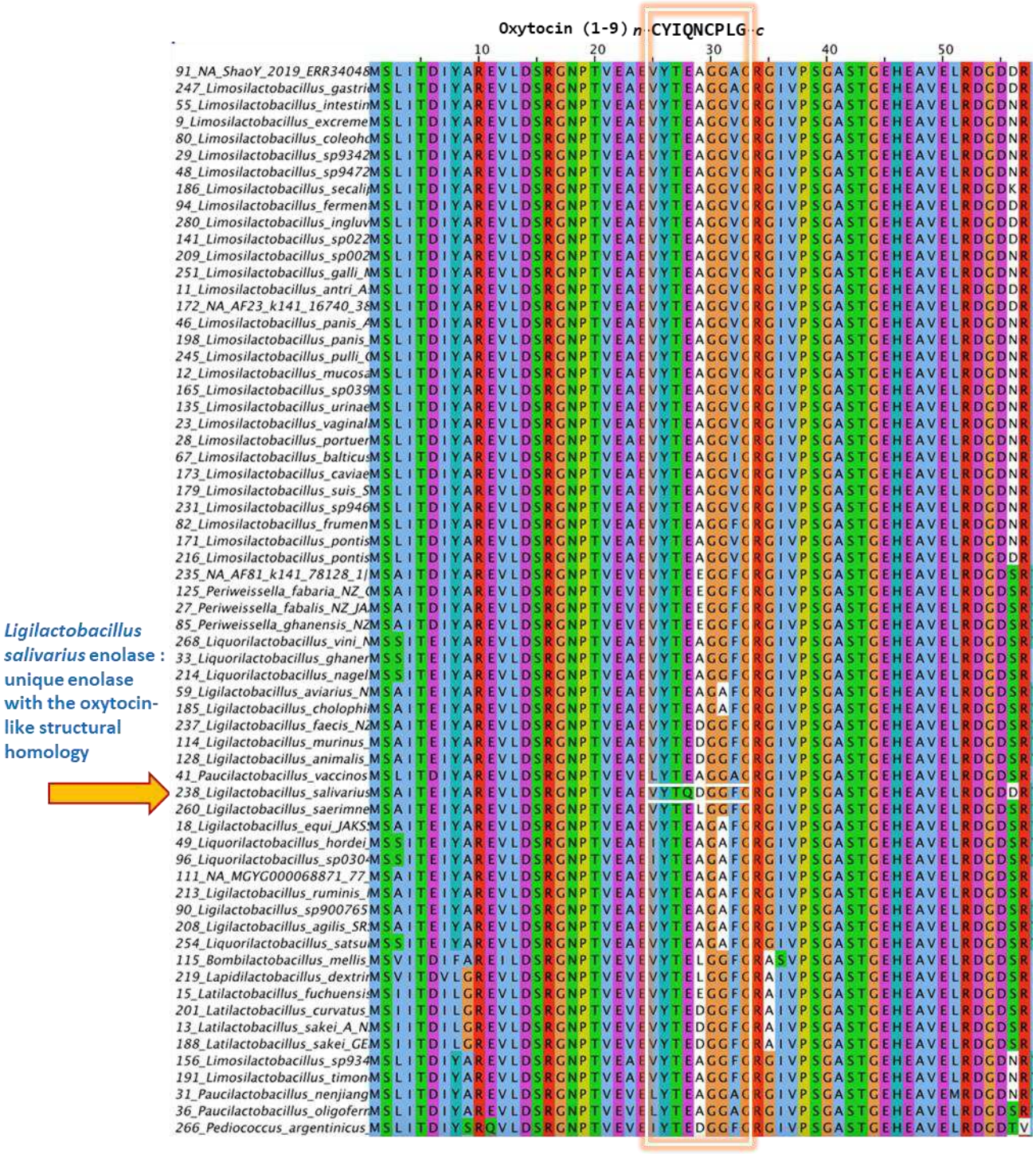
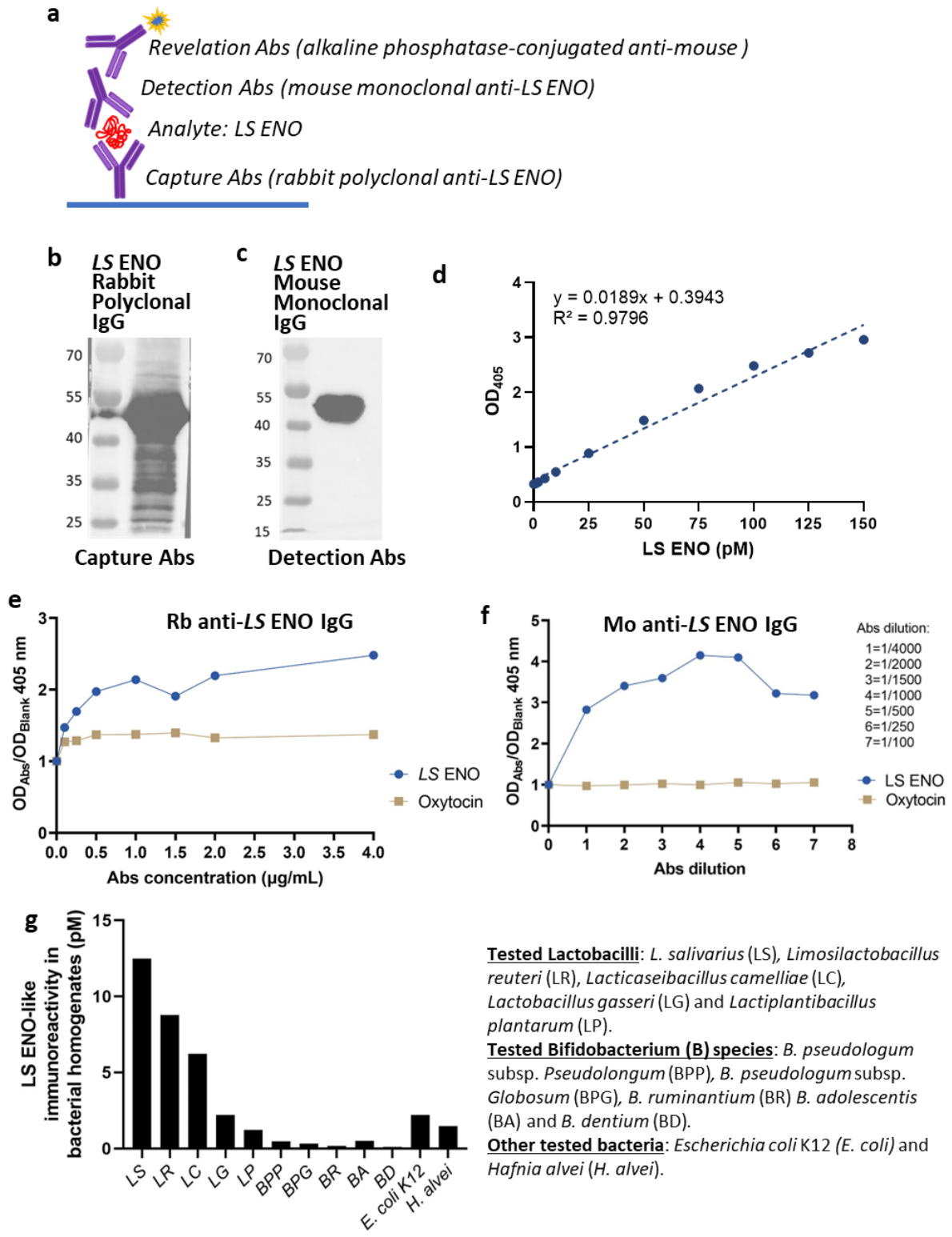


Figure S5. Multiple sequence alignment of oxytocin with enolase from different species of the *Lactobacillaceae* family. Alignment of 283 enolase candidates from 244 human-associated *Lactobacillaceae* species. The candidates were identified from 191.704 high-quality filtered genomes/MAGs retrieved from various genome databases. The figure shows a detailed view of the N-terminal region (first 60 amino acids), containing the OT-like motif, highlighted by a white box. The region displaying sequence similarity with OT was found exclusively in the *LS* enolase sequence. The complete sequence alignment of the 287 enolases is available as a Jalview in: Extended_Data_Figure_S5_Lactobacillaceae_enolases.html.



1171

1172 **Figure S6. Development and validation of ELISA for the in vitro quantification of *LS* ENO. a**. Schematic
1173 representation of the *LS* ENO sandwich ELISA. **b,c**. Western blot validation of anti-*LS* ENO polyclonal (**b**) and
1174 monoclonal (**c**) antibodies used for the capture and detection of *LS* ENO, respectively. **d**. Standard curve of *LS*
1175 ENO detection obtained using the colorimetric assay. **e,f.** Signal-to-background ratios obtained as a function
1176 of the concentration of anti-*LS* ENO capture (**e**) and detection (**f**) antibodies, for testing antibody cross-
1177 reactivity with oxytocin. While an increase in antibody concentration leads to increased *LS* ENO detection
1178 before reaching the plateau, it does not detect oxytocin, confirming the absence of cross-reactivity. **g.** Testing
1179 for *LS* ENO immunoreactivity in protein extracts from different bacterial species as specified in the figure.

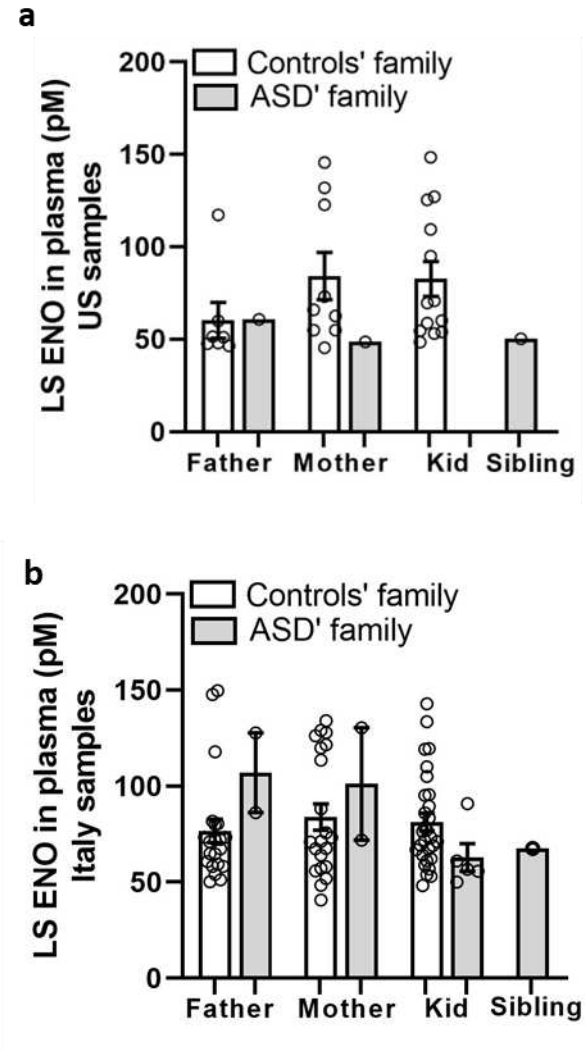


Figure S7. *LS* ENO levels in the GEMMA human cohort. *LS* ENO levels measured in plasma samples from participants of the GEMMA human cohort from the United States (**a**) and Italy (**b**). Each cohort included control and autism spectrum disorder (ASD) families. The family-based cohort design included the father, mother, kid, and siblings within the same family.

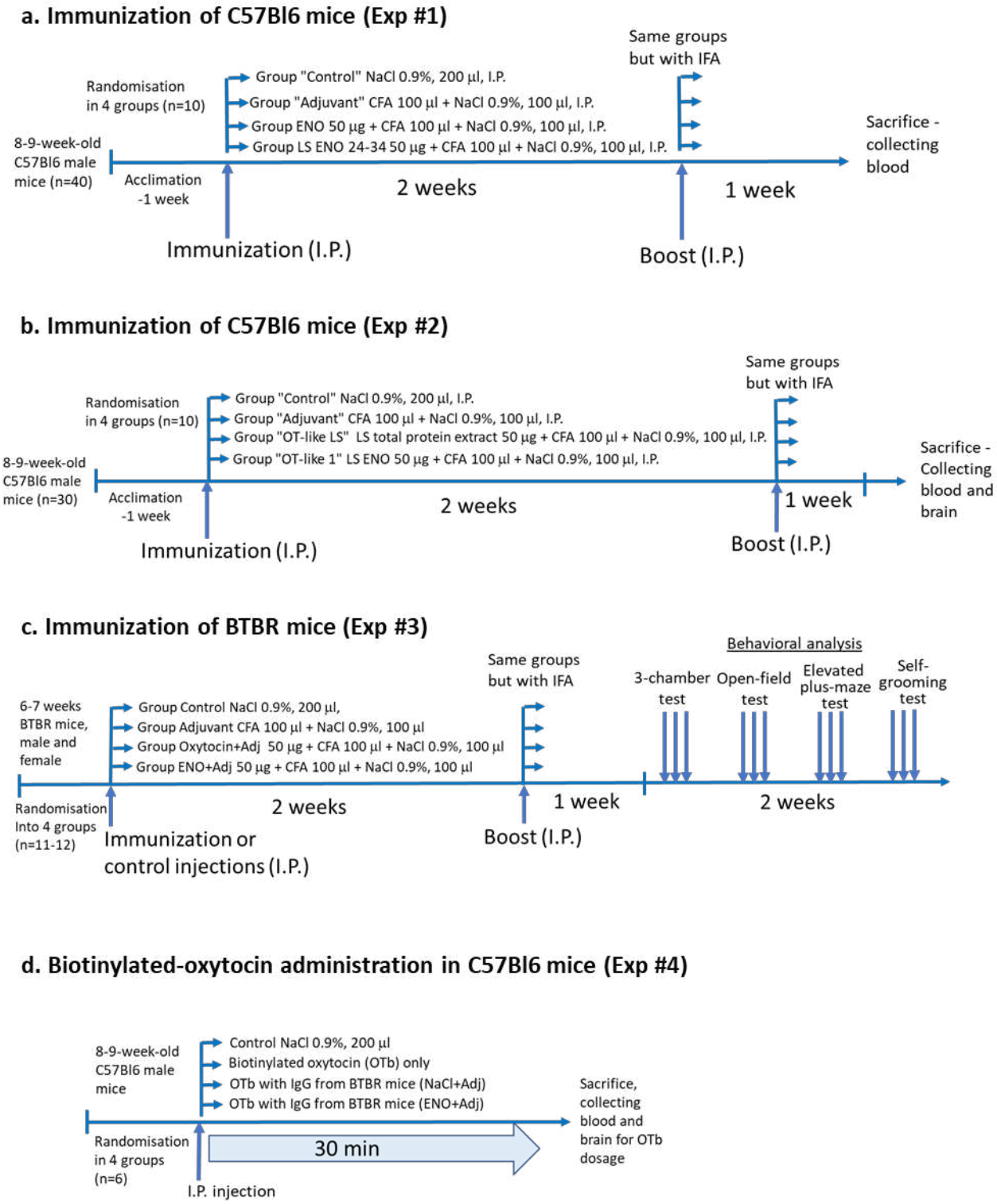


Figure S8. Experimental design of animal studies. Schematic representation of the four experimental protocols performed to investigate the effects of immunization with OT-like proteins. Experiments (Exp) #1, 2, and 4 were conducted in C57BL/6 mice (**a,b,d**), whereas Exp #3 was performed in BTBR mice (**c**). In Exp #1, 2, and 3, mice were immunized with *LS* ENO. Exp #4 was performed in C57 Bl6 mice to investigate whether IgG generated by *LS* ENO immunization of BTBR mice in Exp #3 could influence the transport of peripheral OT to the brain using biotinylated OT (OTb).

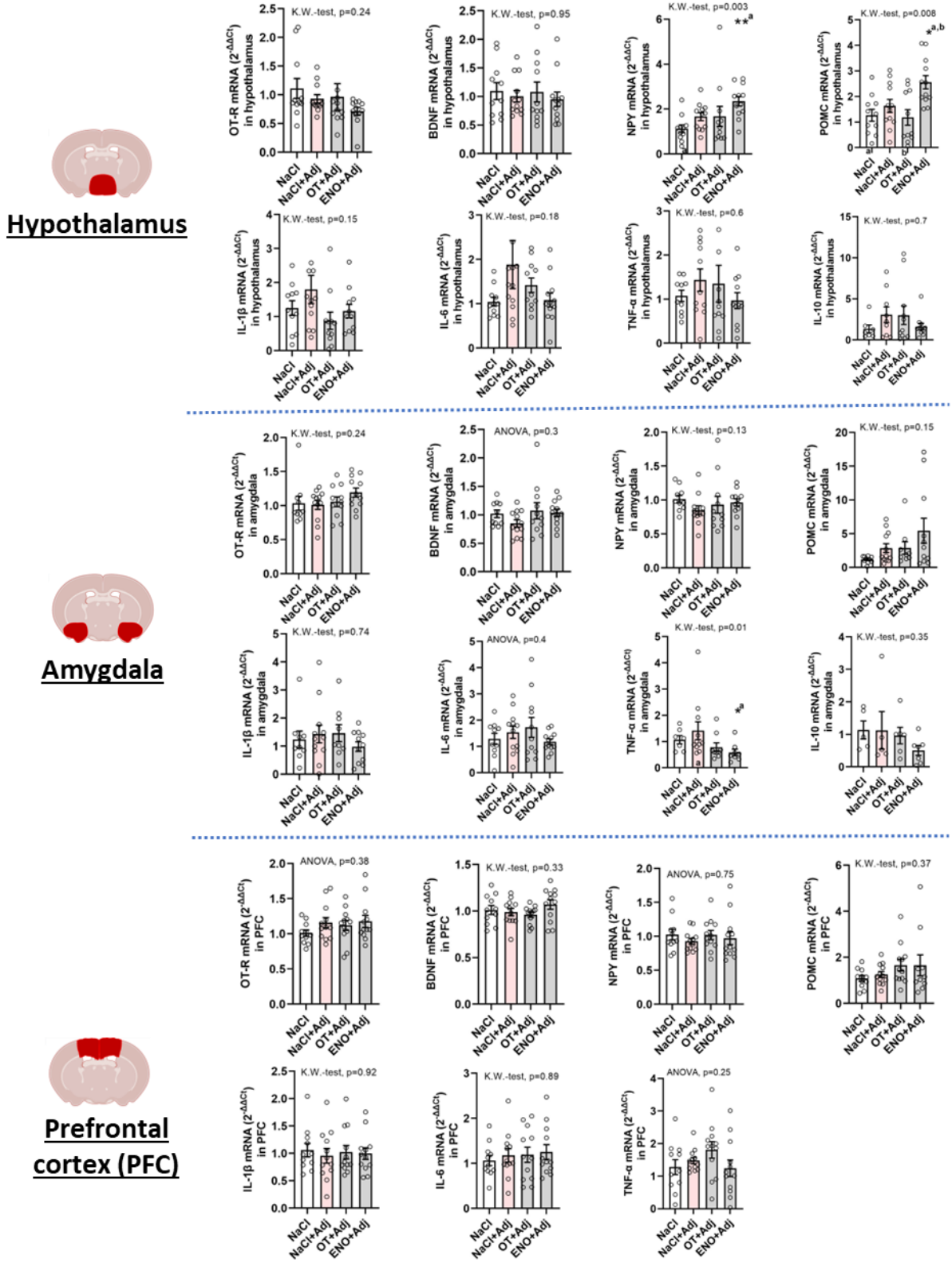


Figure S9. Effects of immunization on the expression of OT-R, regulatory peptides, and cytokines in the brain of BTBR mice. Levels of mRNA expression of oxytocin receptor (OT-R), brain-derived neurotrophic factor (BDNF), neuropeptide Y (NPY), proopiomelanocortin (POMC), interleukin-1β (IL-1β), interleukin-6 (IL-6), tumor necrosis factor-α (TNF-α), and interleukin-10 (IL-10) in the hypothalamus, amygdala, and prefrontal cortex (PFC) of BTBR mice following immunization with OT-like proteins, as assessed by quantitative real-time PCR (qPCR). Statistical analyses were performed using ANOVA or Kruskal-Wallis's test according to the distribution of the data, followed by the appropriate post-hoc test. *p < 0.05, **p < 0.01.

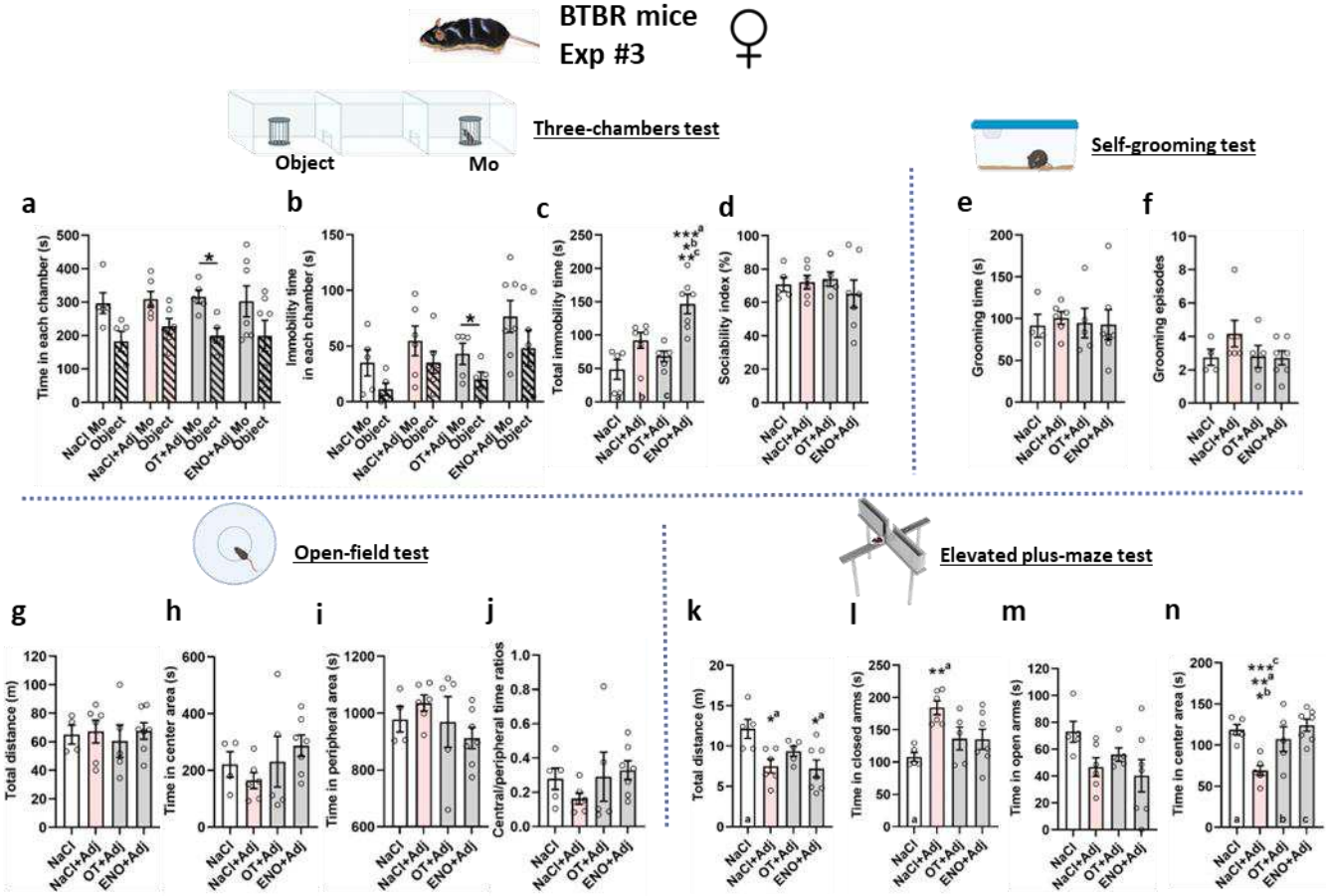


Figure S10. Effect of *LS* ENO immunization on ASD-like behavior in BTBR female mice. Analysis in four groups of female mice receiving saline (NaCl), saline + adjuvants (NaCl+Adj), OT+Adj and *LS* ENO+Adj, respectively. **a-d**. Three-chamber test including time (**a**) and immobility (**b**) spent in the chamber with a stimulus mouse (Mo) or with an Object. **c.** Total immobility time and **d.** Sociability index. **e,f.** Self-grooming test, including grooming time (**e**) and number of grooming episodes (**f**). **g-j.** Open-field test, including total distance traveled (**g**), time spent in the center (**h**) and peripheral (**i**) areas, as well as their ratios (**j**). **k-n.** Elevated plus-maze test, including total distance traveled (**k**), time spent in closed (**l**) and in open (**m**) arms, as well as in the center area (**n**). **a,b,** Paired Wilcoxon's tests *p<0.05. **c,** ANOVA, p=0.0007, Tukey's post-test *p<0.05, **p<0.01. **k,** ANOVA, Tukey's post-test *p<0.05. **l,** ANOVA, Tukey's post-tests **p<0.01.

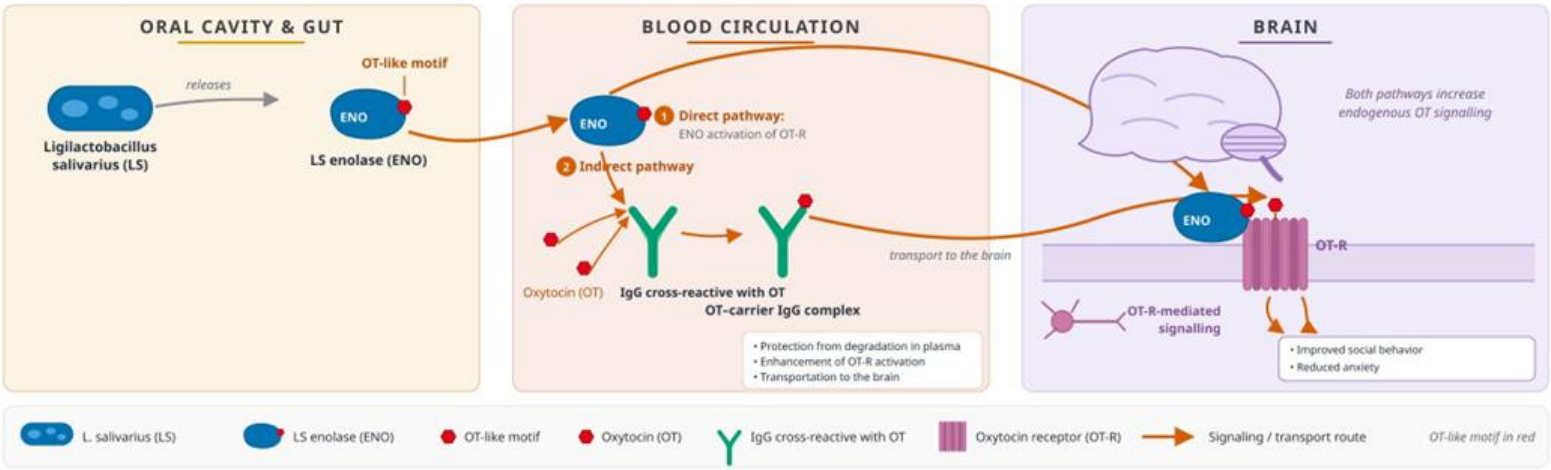
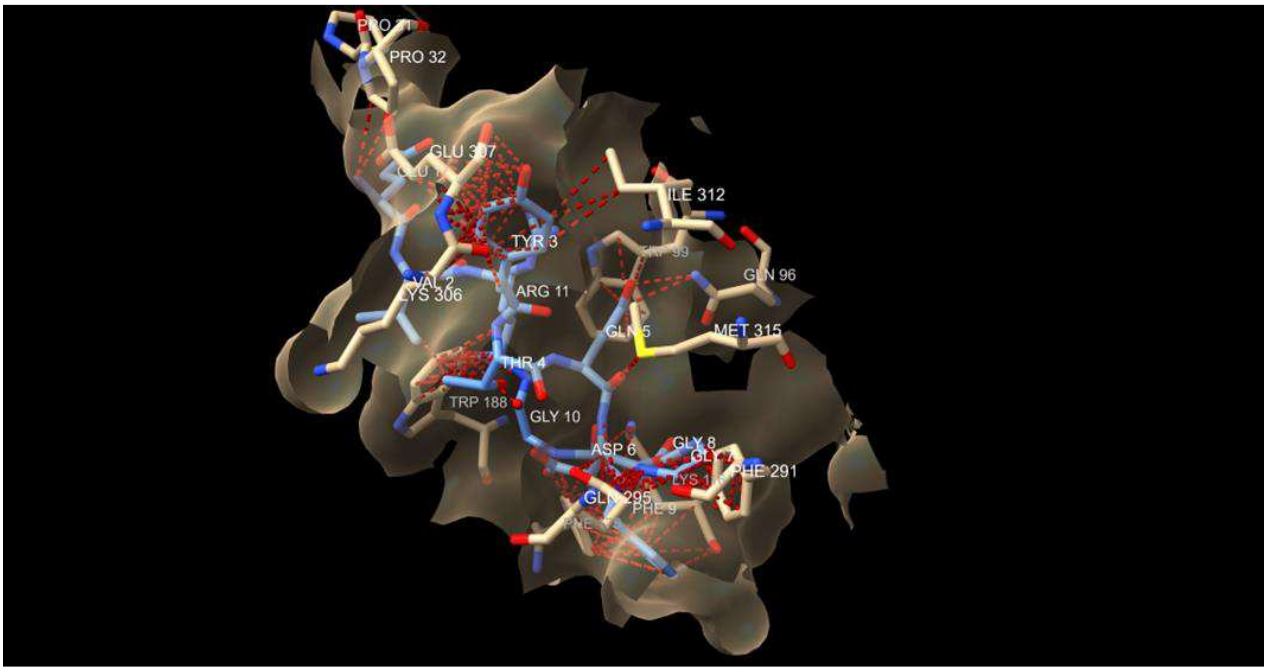
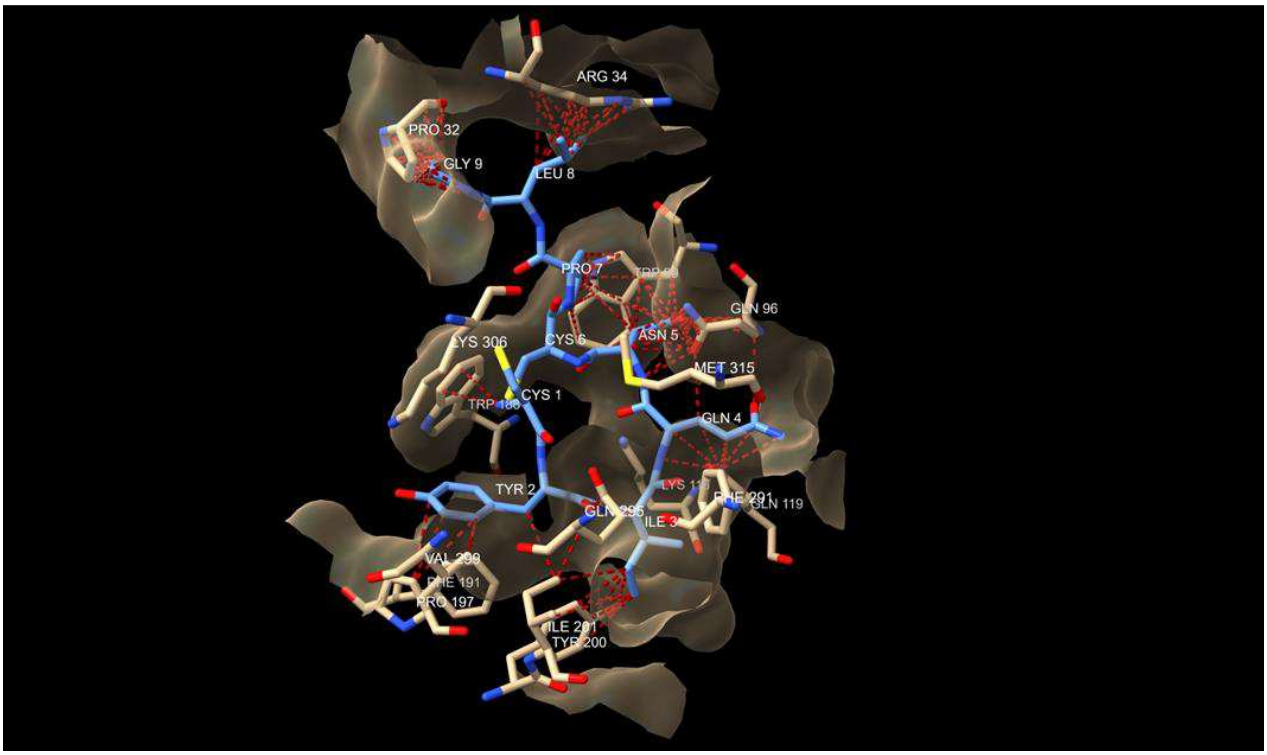


Figure S11. Schematic summary of the discovered link between *Ligilactobacillus* salivarius (*LS)* enolase (ENO) and the host oxytocin (OT) signaling. Produced by *LS* present in the oral cavity and gut, *LS* ENO reaches the systemic circulation and was also detected in the brain. Two signaling pathways are present, direct *LS* ENO activation of the oxytocin receptor (OT-R) as a weak ligand and, indirect, in which *LS* ENO plays a role of OT-like antigen to stimulate production of IgG cross-reactive with OT, which will enhance endogenous OT signaling by acting as an OT-carrier protein. Both pathways should increase OT-R-mediated signaling in the brain, leading to improvement of social behavior and reduction of anxiety, although the contribution of the direct pathway needs further elucidation. OT-like motif in the *LS* ENO protein is depicted in red. Figure generated with the help of Vibe (Mistral AI) based on an original drawing.

a. ***LS*** **ENO (24-34)** **GLU 1- VAL 2- TYR 3- THR 4- GLN 5- ASP 6- GLY 7- GLY 8- PHE 9- GLY 10- ARG 11**



b. **Oxytocin** **CYS 1- TYR 2- ILE 3- GLN 4- ASN 5- CYS 6- PRO 7- LEU 8- GLY 9**



1241

1242 **Figure S12. AlphaFold modeling of the OT-like *LS* ENO (24-34) fragment and oxytocin binding to the oxytocin**
1243 **receptor. a**. Predicted binding of the *LS* ENO (24-34) peptide. **b**. Predicted binding of oxytocin. *LS* ENO (24-34)
1244 fragment binds to the same with OT OT-R binding pocket as shown by three identical amino acids of the OT-R
1245 (GLN 96, LYS 306 and MET 315) interacting with both ligands. However, TYR 2 and GLN 4 from OT and the
1246 homologous TYR 3 and GLN 5 from the *LS* ENO fragment establish contacts with different amino acids of the
1247 receptor, probably underlying a weaker potency of the bacterial protein fragment to activate OT-R. The binding
1248 pocket of OT-R is shown as a gray cloud. Atomic contacts between the ligands (shown in blue) and the OT-R
1249 structure (shown in light grey) were identified using a Van Der Waals overlap threshold of ≥ -0,4 Å in UCSF
1250 ChimeraX and are depicted as red dashed lines. Modeling was performed using AlphaFold2 online program
1251 (https://colab.research.google.com/github/sokrypton/ColabFold/blob/main/AlphaFold2.ipynb).

Supplementary Files

This is a list of supplementary files associated with this preprint. Click to download.

- GEMMAConsortiumlist.docx